CR-203634

IN-90
51 P.

ADP RESEARCH STUDIES

Purchase Order No. S-30917-F
FINAL REPORT

prepared for
NASA/Goddard Space Flight Center

prepared by
Computer Sciences Corporation

Title: International AGN Watch: Continuous Monitoring of NGC 4151

PI: D.M. Crenshaw

Statement of Work:

This work supports an approved IUE program that represents the most intense UV monitoring campaign of a Seyfert galaxy to date. The goals of the ADP program are to measure the ~400 spectra, perform basic time-series analyses, and write and publish the initial paper so that the data can be used for additional detailed studies.

Results:

The results of this project are reported in a ~40 page manuscript with over 80 co-authors to be submitted to the Astrophysical Journal. The nucleus of NGC 4151 was observed continuously with the *International Ultraviolet Explorer* (IUE) for 9.3 days, yielding a pair of LWP and SWP spectra every ~70 minutes, and during four-hour periods for 4 days prior to and 5 days after the continuous monitoring period. The sampling frequency of the observations is an order of magnitude higher than that of any previous UV monitoring campaign on a Seyfert galaxy.

The continuum fluxes in bands from 1275 Å to 2688 Å went through four significant and well-defined "events" of duration 2 – 3 days during the continuous monitoring period. We find that the amplitudes of the continuum variations decrease with increasing wavelength, which extends a general trend for this and other Seyfert galaxies to smaller time scales (i.e., a few days). Cross-correlation analysis shows that the continuum variations in all of the UV bands are *simultaneous* to within ±0.1 days, providing a strict constraint on continuum models. The emission-line light curves show only one major event during the continuous monitoring (a slow rise followed by a shallow dip), and do not correlate well with continuum light curves over the (short) duration of the campaign, because the time scale for continuum variations is apparently smaller than the response time of the emission lines.

Publications:

"Multiwavelength Observations of Short Time-Scale Variability in NGC 4151. I. Ultraviolet Observations", Crenshaw, D.M., Rodriguez-Pascual, P.M., Penton, S.V., Edelson, R.A., et al. 1995, to be submitted to the ApJ.

MULTIWAVELENGTH OBSERVATIONS OF SHORT TIME-SCALE VARIABILITY IN NGC 4151. I. ULTRAVIOLET OBSERVATIONS

D.M. Crenshaw,[1] P.M. Rodríguez-Pascual,[2] S.V. Penton,[3] R.A. Edelson,[4] D. Alloin,[5] T.R. Ayres,[3] J. Clavel,[6] K. Horne,[7] W.N. Johnson,[8] S. Kaspi,[9] K.T. Korista,[10] G.A. Kriss,[11] J.H. Krolik,[11] M.A. Malkan,[12] D. Maoz,[9] H. Netzer,[9] P.T. O'Brien,[13] B.M. Peterson,[14] G.A. Reichert,[15] J.M. Shull,[3,16] M.-H. Ulrich,[17] W. Wamsteker,[2] R.S. Warwick,[18] T. Yaqoob,[19] T.J. Balonek,[20] P. Barr,[6] G.E. Bromage,[21] M. Carini,[22] T.E. Carone,[23] F.-Z. Cheng,[24] K.K. Chuvaev,[25] M. Dietrich,[26] V.T. Doroshenko,[27] D. Dultzin-Hacyan,[28] A.V. Filippenko,[29] C.M. Gaskell,[30] I.S. Glass,[31] M.R. Goad,[32] J. Hutchings,[33] D. Kazanas,[19] W. Kollatschny,[34] A.P. Koratkar,[32] A. Laor,[35] K. Leighly,[36] V.M. Lyutyi,[37] G.M. MacAlpine,[38] Yu.F. Malkov,[25] P.G. Martin,[39] B. McCollum,[22] N.I. Merkulova,[25] L. Metik,[25] V.G. Metlov,[27] H.R. Miller,[40] S.L. Morris,[33] V.L. Oknyanskij,[25,41] J. Penfold,[42] E. Pérez,[43] G.C. Perola,[44] G. Pike,[45] R.W. Pogge,[14] I. Pronik,[25] V.I. Pronik,[25] R.L. Ptak,[46] M.C. Recondo-González,[2] J.M. Rodríguez-Espinoza,[47] E.L. Rokaki,[48] J. Roland,[49] A.C. Sadun,[50] I. Salamanca,[5] M. Santos-Lleó,[5] J. Sanz,[2] S.G. Sergeev,[25] S.M. Smith,[14] M.A.J. Snijders,[51] L.S. Sparke,[52] G.M. Stirpe,[53] R.E. Stoner,[46] W.-H. Sun,[54] E. van Groningen,[41] R.M. Wagner,[14,55] S. Wagner,[26] I. Wanders,[14] W.F. Welsh,[56] R.J. Weymann,[57] B.J. Wilkes,[58] and W. Zheng[11]

Received ______________________

[1]Computer Sciences Corporation, Laboratory for Astronomy and Solar Physics, NASA Goddard Space Flight Center, Code 681, Greenbelt, MD 20771.

[2]ESA IUE Observatory, P.O. Box 50727, 28080 Madrid, Spain.

[3]Center for Astrophysics and Space Astronomy, University of Colorado, Campus Box 389, Boulder, CO 80309.

[4]Department of Physics and Astronomy, University of Iowa, Iowa City, IA 52242.

[5]Observatoire de Paris, URA 173 CNRS, 92195 Meudon, France.

[6]ISO Observatory, Astrophysics Division of ESA, ESTEC, Postbus 299, 2200-AG, The Netherlands.

[7]School of Physics and Astronomy, University of St. Andrews, North Haugh, St. Andrews KY16 9SS, Scotland, United Kingdom.

[8]Naval Research Laboratory, Code 4151, 4555 Overlook SW, Washington, DC 20375-5320.

[9]School of Physics and Astronomy and the Wise Observatory, The Raymond and Beverly Sackler Faculty of Exact Sciences, Tel-Aviv University, Tel-Aviv 69978, Israel.

[10]Department of Physics and Astronomy, University of Kentucky, Lexington, KY 40506.

[11]Department of Physics and Astronomy, The Johns Hopkins University, Baltimore, MD 21218.

[12]Department of Astronomy, University of California, Math-Science Building, Los Angeles, CA 90024.

[13]Department of Astrophysics, Oxford University, Keble Road, Oxford OX1 3RH, United Kingdom.

[14]Department of Astronomy, The Ohio State University, 174 West 18th Avenue, Columbus, OH 43210.

[15]Universities Space Research Association, NASA Goddard Space Flight Center, Code 668, Greenbelt, MD 20771.

[16]Joint Institute for Laboratory Astrophysics: University of Colorado and National Institute of Standards and Technology, Campus Box 440, Boulder, CO 80309.

[17]European Southern Observatory, Karl Schwarzschild Strasse 2, 85748 Garching, Germany.
[18]Department of Astronomy, University of Leicester, University Road, Leicester LE1 7RH, United Kingdom
[19]Laboratory for High Energy Astrophysics, Code 665, NASA Goddard Space Flight Center, Greenbelt, MD 20771.
[20]Department of Physics and Astronomy, Colgate University, Hamilton, NY 13346.
[21]Centre for Astrophysics, University of Central Lancashire, Preston PR1 2HE, U.K.
[22]Computer Sciences Corporation, NASA Goddard Space Flight Center, Code 684.9, Greenbelt, MD 20771.
[23]Space Sciences Laboratory, University of California, Berkeley, CA 94720, and Eureka Scientific, Inc.
[24]Center for Astrophysics, University of Science and Technology, Hefei, Anhui, People's Republic of China.
[25]Crimean Astrophysical Observatory, P/O Nauchny, 334413 Crimea, Ukraine.
[26]Landessternwarte, Königstuhl, D-69117 Heidelberg, Germany.
[27]Sternberg State Astronomical Institute, P/O Nauchny, 334413 Crimea, Ukraine.
[28]Universidad Nacional Autonoma de Mexico, Instituto de Astronomia, Apartado Postal 70-264, 04510 Mexico D.F., Mexico.
[29]Department of Astronomy, University of California, Berkeley, CA 94720.
[30]Department of Physics and Astronomy, University of Nebraska, Lincoln, NE 68588.
[31]South African Astronomical Observatory, P.O. Box 9, Observatory 7935, South Africa.
[32]Space Telescope Science Institute, 3700 San Martin Drive, Baltimore, MD 21218.
[33]Dominion Astrophysical Observatory, 5071 West Saanich Road, Victoria, B.C. V8X 4M6, Canada.
[34]Universitäts-Sternwarte Göttingen, Geismarlandstrasse 11, D-37083 Göttingen, Germany.
[35]Department of Astronomy, Caltech 130-33, Pasadena, CA 91125.
[36]Cosmic Radiation Laboratory, RIKEN, Hirosawa 2-1, Wako, Saitama 351, Japan.
[37]Sternberg Astronomical Institute, University of Moscow, Universitetskij Prosp. 13, Moscow 119899, Russia.
[38]Department of Astronomy, University of Michigan, Dennison Building, Ann Arbor, MI 48109.
[39]Canadian Institute for Theoretical Astrophysics, University of Toronto, Toronto, ON M5S 1A1, Canada.
[40]Department of Physics and Astronomy, Georgia State University, Atlanta, GA 30303.
[41]Astronomiska observatoriet, Box 515, S-751 20 Uppsala, Sweden.
[42]Department of Physics and Astronomy, University of Calgary, 2500 University Drive NW, Calgary, AB T2N 1N4, Canada, and Department of Mathematics, Physics, and Engineering, Mount Royal College, Calgary T3E 6K6, Canada.
[43]Instituto de Astrofisica de Andalucia, Aptdo. 3004, 18080 Granada, Spain.
[44]Istituto Astronomico dell'Università, Via Lancisi 29, I-00161 Rome, Italy.
[45]Pike
[46]Department of Physics and Astronomy, Bowling Green State University, Bowling Green, OH 43403.
[47]Instituto de Astrofísica de Canarias, E-38200 La Laguna, Tenerife, Spain.
[48]Royal Observatory Edinburgh, University of Edinburgh, Blackford Hill, Edinburgh EH9 3HJ, United Kingdom.
[49]Institut d'Astrophysique, 98 bis Boulevard Arago, F-75014 Paris, France.
[50]Department of Physics and Astronomy and Bradley Observatory, Agnes Scott College, Decatur, GA 30030.
[51]IRAM, 300 Rue de la Piscine, 38046 Saint Martin d'Heres, France.
[52]Department of Astronomy, University of Wisconsin, 475 N. Charter Street, Madison, WI 53706.
[53]Osservatorio Astronomico di Bologna, Via Zamboni 33, I-40126, Bologna, Italy.
[54]Institute of Astronomy, National Central University, Chung-Li, Taiwan 32054, Republic of China.
[55]Mailing address: Lowell Observatory, Mars Hill Road, 1400 West, Flagstaff, AZ 86001.
[56]Department of Physics, Keele University, Keele ST5 5BG, Staffordshire, United Kingdom.
[57]Observatories of the Carnegie Institution of Washington, 813 Santa Barbara Street, Pasadena, CA 91101.
[58]Harvard-Smithsonian Center for Astrophysics, 60 Garden Street, Cambridge, MA 02138.

ABSTRACT

We present the results of an intensive ultraviolet monitoring campaign on the Seyfert 1 galaxy NGC 4151, as part of an effort to study its short time-scale variability over a broad range in wavelength. The nucleus of NGC 4151 was observed continuously with the *International Ultraviolet Explorer* (IUE) for 9.3 days, yielding a pair of LWP and SWP spectra every ~70 minutes, and during four-hour periods for 4 days prior to and 5 days after the continuous monitoring period. The sampling frequency of the observations is an order of magnitude higher than that of any previous UV monitoring campaign on a Seyfert galaxy.

The continuum fluxes in bands from 1275 Å to 2688 Å went through four significant and well-defined "events" of duration 2 – 3 days during the continuous monitoring period. We find that the amplitudes of the continuum variations decrease with increasing wavelength, which extends a general trend for this and other Seyfert galaxies to smaller time scales (i.e., a few days). Cross-correlation analysis shows that the continuum variations in all of the UV bands are *simultaneous* to within ±0.1 days, providing a strict constraint on continuum models. The emission-line light curves show only one major event during the continuous monitoring (a slow rise followed by a shallow dip), and do not correlate well with continuum light curves over the (short) duration of the campaign, because the time scale for continuum variations is apparently smaller than the response time of the emission lines.

Subject headings: galaxies: individual (NGC 4151) – galaxies:active – galaxies:Seyfert – ultraviolet:spectra

1. Introduction

Variability monitoring of active galactic nuclei (AGN) has become the most productive way to probe the spatially unresolved nuclear continuum source and, when present, surrounding broad-line region (BLR). The success of recent large-scale monitoring campaigns are due to high temporal sampling rates over extended periods of time (see Peterson 1993 for a review). The cornerstone of most of these campaigns has been the International Ultraviolet Explorer (IUE), because it can provide long periods of observations at precise intervals, accurate absolute flux levels, and access to the UV, where the continuum and high-ionization lines are more strongly variable than in the optical. Most campaigns have focused on nearby bright Seyfert 1 galaxies whose UV continua and emission lines were previously known to be strongly variable.

The initial IUE campaign on NGC 5548 is described by Clavel et al. (1991), and results from concurrent and subsequent ground-based monitoring programs are given in Peterson et al. (1991, 1992, 1994), and Dietrich et al. (1993). One of the most fundamental results from these efforts is that there was no detectable delay between the variations in the ultraviolet continuum bands and those in the optical; that is, the time lag between the UV and optical light curves was ≤ 4 days (the sampling interval for the IUE campaign). This provides an important constraint on models of the continuum source. For example, for thin accretion disks (e.g., Shakura & Sunyaev 1973), this implies that surprisingly high radial signal speeds ($\gtrsim 0.1c$) coordinate the different regions of the disk (Krolik et al. 1991). A possible explanation is that the UV and optical continuum emission is due to reprocessing by cooler, outer material of X-ray photons created closer in (Courvoisier & Clavel 1991; Collin-Souffrin 1991; Krolik et al. 1991).

A major campaign on NGC 3783 with IUE (Reichert et al. 1994) and ground-based telescopes (Stirpe et al. 1994) resulted in the same approximate upper limit (± 4 days) for the lag between optical and UV continuum variations. A subsequent HST, IUE, and ground-based campaign on NGC 5548 (Korista et al. 1995), anchored by daily observations with the Faint Object Spectrograph, demonstrated that the UV and optical continuum variations in NGC 5548 were further constrained to be simultaneous to within ±1 day. In addition, Clavel et al. (1992) show that the X-ray and UV continuum fluxes are correlated, but with considerable scatter and a rather loose constraint of ≤ 6 days on the time lag. In order to obtain tighter constraints on the lags, if any, between X-ray, UV, and optical continuum variations, it became evident that a multiwavelength monitoring project with even higher temporal resolution was needed.

The previous campaigns have also demonstrated that the emission-line response times to changes in the photoionizing continuum are very short (days) and a function of ionization, with the high ionization lines responding more rapidly. In fact, the initial campaigns on NGC 5548 and NGC 3783 (Clavel et al. 1991; Reichert et al. 1994) found that the lags for the highest ionization lines, He II λ1640 and N V λ1240, were unresolved (i.e., ≤ 4 days). With the higher sampling of the subsequent HST, IUE, and ground-based campaign on NGC 5548, Korista et al. (1995) were able to determine that the lags for these lines were slightly less than 2 days. Thus, a secondary goal for obtaining higher temporal resolution is to check this result for this and other Seyferts, and specifically to fully resolve the transfer function of the high ionization lines (Peterson 1993).

A new effort was initiated to provide an order of magnitude increase in the sampling rate over previous campaigns on Seyfert 1 galaxies, similar to that obtained for the BL LAC object PKS 2155–304, which was monitored continuously by IUE for 5 days (Urry et al. 1993) as part of a multiwavelenth campaign (Edelson et al. 1995). A determined effort was also made to obtain concurrent observations of NGC 4151 at other wavelengths, particularly in the optical X-ray regions, to test the predictions of accretion disk and continuum reprocessing models. This would also allow a comparison with the multiwavelength observations of PKS 2155-304, an object with a strong *beamed* component. The data and basic results from the IUE campaign on NGC 4151 are given in this paper. Other papers in this series report on optical observations (Kaspi et al. 1995. Paper II). high-energy observations (Warwick et al. 1995. Paper III). and a comparison of the multiwavelength continuum data (Edelson et al. 1995b. Paper IV).

NGC 4151 is a nearby ($cz = 995$ km s^{-1}) barred spiral galaxy that is viewed nearly face-on (Simkin 1975). It was classified as a Seyfert 1.5 by Osterbrock & Koski (1976). because its nucleus shows strong narrow components for the permitted lines. in addition to the broad (thousands of km s^{-1} FHWM) permitted and narrow (hundreds of km s^{-1} FWHM) forbidden lines that define a Seyfert 1 galaxy. HST images show that the narrow-line [O III] $\lambda5007$ emission arises from a nuclear point source and an extended ($\sim 3''$) NLR that consists of a number of emission-line clouds in a biconical structure (Evans et al. 1993). The radio emission is extended along the same general direction as the [O III] emission on arcsecond and sub-arcsecond scales (Johnston et al. 1982; Wilson and Ulvestad 1983), although the optical emission-line and radio axes are misaligned by $\sim 20°$. NGC 4151 exhibits a complex X-ray spectrum. which can be characterized in the 2 - 10 keV region by a power-law continuum modified by a warm or partial absorber. and in addition. a soft X-ray excess in the 0.1 - 2 keV range (Holt et al. 1980; Yaqoob. Warwick. and Pounds 1989; Weaver et al. 1994a,b).

Because it is so bright and strongly variable in the UV. NGC 4151 is the ideal target for intensive monitoring (see Ulrich et al. 1991 for a summary of previous UV observations). It shows ultraviolet continuum variations with doubling times as short as a week (Clavel et al. 1990), and is one of the few AGN for which emission-line cross-correlation lags have been reliably determined, yielding characteristic time scales for emission-line response of 4 ± 3 days for C IV $\lambda1549$ (Clavel et al. 1990) and 9 ± 2 days for the Balmer lines (Maoz et al. 1991). The UV spectrum of NGC 4151 shows extremely broad emission lines (~30.000 km s^{-1} FWZI for C IV). It also contains a number of broad (1000 km s^{-1}), blue shifted (-1100 to -100 km s^{-1}). and variable absorption lines that arise in ions of widely different stages (Bromage et al. 1985; Kriss et al. 1992), and two unidentified emission lines, known as L1 λ1518 and L2 λ1594, that bracket the C IV λ1549 feature (Ulrich et al. 1985; Clavel et al. 1987).

2. Observations

The nucleus of NGC 4151 was observed with the IUE SWP (1150 - 1970 Å) and LWP (1970 - 3300 Å) cameras through the large apertures (10″x 20″) in low-dispersion mode (resolution = 5 - 8 Å FWHM). Observations were made in a continuous mode over 9.3 days during 1993 December 1 – 10. In addition, observations were obtained during four-hour US2 shifts (which frequently experience higher particle radiation) on the four days prior to and five days after the continuous monitoring period. The standard observing procedure was to obtain alternate LWP and SWP exposures by reading and preparing one camera while the other camera was exposing, which resulted in a pair of spectra every ~70 minutes. During each day of the continuous monitoring, the observations were interupted for ~2 hours as the Earth occulted the target and the spacecraft was maneuvered to a low β (angle between the telescope axis and the anti-solar direction) to maintain attitude control and cool the onboard computer.

The observations were affected by the presence of scattered solar (and occasionally Earth) light in the telescope tube, which has been present since early 1991 and is strong at $\beta \geq 50$ (Carini & Weinstein 1992). In order to obtain concurrent observations with other satellites (e.g., ROSAT) it was necessary to observe NGC 4151 at $\beta \approx 90°$. The scattered light spectrum is such that there is contamination of the LWP spectra at the long-wavelength end (see section 3.2), but no contamination of the SWP spectra. The most noticeable effect of the scattered light is that it greatly increases the background level in the FES, which is the optical target acquisition detector. Thus, the nucleus of NGC 4151 could not be detected directly, since the

FES background counts exceeded those expected for the target by a factor of ~50, and no optical light curve could be obtained from the FES. Fortunately, the scattered light had little effect on acquisition and guiding during the exposures. The nucleus of NGC 4151 was acquired by blind offset from a nearby bright star (SAO 62869), which is a procedure that typically results in a positioning error in the aperture that is < 1″. During the exposures, the same bright star was used for guiding, since it remained in the portion of the FES field-of-view that is least affected by the scattered light. The offset slew was repeated about once every 8 hours to recenter the target in the aperture and to update the guide star position, since the spacecraft rolls to maintain optimal positioning of the solar arrays.

A log of the IUE observations is given in Table 1. The UT date, start time, and duration are given, along with the Julian Date for the *midpoint* of each exposure. The exposure levels from the raw images, as determined by the telescope operators at the time of the observations, are given in Data Numbers (DN), where a value of 255 indicates overexposure. Athough the determination of the exposure levels is somewhat subjective, they are accurate enough to evaluate the general quality of the data. The emission levels are given for the peak of C IV (SWP) or Mg II (LWP), and the continuum and background levels are averages of values in the long-wavelength region of each camera. Exposure levels were not available for a couple of images that had to be recovered from analog tape. The exposure levels are all considered to be near optimal, except for the few images flagged in the notes. There was significant particle radiation for some of the images obtained during the US2 shifts, which could result in slightly lower signal-to-noise ratios for the affected spectra; these spectra can be identified by background levels that are substantially higher than the average background levels, which are typically ~15 DN for the SWP and ~27 DN for the LWP.

A total of 205 SWP and 196 LWP spectra were obtained of NGC 4151 during the campaign.

Only six images are considered to be unusable. The exposure time for SWP 49394 was cut short due to an impending Earth occultation. The target was on the edge of the aperture for LWP 26984, SWP 49428, and LWP 26895. Most of the two images for LWP 26931 and LWP 27008 were lost due to telemetry problems, and could not be recovered. The other problems in the notes for Table 1 are minor, and do not significantly affect the measured fluxes: the microphonics are a periodic noise pattern with an amplitude ≤ 8 DN (Newmark et al. 1992) that occur infrequently, and the additional 10 minutes of exposure in high-dispersion for LWP 27024 had no detectable impact. We are left with 395 useful spectra to work with: 203 SWP and 192 LWP.

3. Data Reduction and Analysis

The IUE project has developed techniques for improving the signal-to-noise, wavelength assignment, and flux calibration of IUE spectra: these techniques are being used in the new processing system (NEWSIPS) to produce the IUE Final Archives. However, at the time of the observations, only the old processing system (IUESIPS) was available for current data. We decided to use a newly available system developed by Tom Ayres called "TOMSIPS".

3.1 TOMSIPS Reduction

TOMSIPS is based on many of the techniques developed for NEWSIPS and includes a realistic noise model (Ayres 1993). TOMSIPS, like NEWSIPS, uses an identically rotated intensity transfer function (ITF). The old IUESIPS used pre-rotated ITFs, which do not always match up with the current image and can introduce fixed pattern noise. TOMSIPS uses an ITF based directly on the raw images of the flux standard white dwarf G191B2B, and a wavelength calibration based upon the emission-line spectra of λ Andromeda.

TOMSIPS uses a slit-weighted extraction method similar to the OPTIMAL techique (Kinney, Bohlin, & Neill 1991), with the distinct difference that the cross-dispersion profile is not of a fixed form, but matches the actual average cross-dispersion profile in the region. Because the cross-dispersion profile is both wavelength and emission-line dependent, 10 separate cross-dispersion regions are used for the SWP and 7 are used for the LWP. Unlike previous extraction techniques, including OPTIMAL and GEX (Gaussian extraction, see Reichert et al. 1994), the TOMSIPS errors are not "extraction" errors, but are true estimates of the flux uncertainties empirically derived from an independent noise model (Ayres 1993). The improved noise model and similarly processed ITF substantially reduces the pixel-to-pixel variations of the final spectra. A detailed comparison of TOMSIPS with other processing techniques appears in Penton et al. (1995).

3.2 Scattered Light Contamination of LWP Spectra

The scattered light in the IUE telescope is characterized by a solar spectrum (Carini & Weinstein 1992), and therefore rises sharply at the long-wavelength end of the LWP region. Unfortunately, the scattered light exhibits a strong (and possibly variable) gradient across the aperture, and there are no proven techniques for removing it at this time. The flux levels of several sky background LWP spectra obtained during the campaign indicate that the scattered light contributed the following approximate percentages to the total fluxes in the continuum bands: ~1% at 2300 Å, ~ 7% at 2688 Å, ~26% at 2970 Å, and ~37% at 3130 Å. Checks of the flux levels inside the aperture, but away from the spectra, indicate that the background contribution typically varied by ≤1% at 2688 Å over the course of a day, presumably as a result of changing β or Earth angle. At longer wavelengths, the background variation started to significantly alter the observed continuum variations.

3.3 Continuum and Line Measurements

Continuum measurements are made in known line-free bands in the rest frame of NGC 4151. A continuum flux is taken to be the error-weighted mean over the bandpass, and the continuum flux error is the standard deviation of the mean over the bandpass. For SWP spectra, the continuum regions selected are 1260 – 1290 Å, 1420 – 1460 Å, and 1805 – 1835 Å. In the LWP spectra, the only usable continuum band is 2625 - 2750 Å: at shorter wavelengths, the spectra are too noisy, and at longer wavelengths, the spectra are too contaminated by the variable scattered light. The continuum bands are shown in Figure 1, along with the average SWP and LWP spectra for this campaign. The sharp upturn at the long-wavelength end is due to the scattered light contamination.

To measure the emission and absorption line components, pre-defined regions around each feature of interest are extracted and a fit is made in the rest frame. Initially, the fit consists of a power-law continuum of the form $F_\lambda = F_0(\lambda/\lambda_0)^\alpha$, with the data weighted by the TOMSIPS errors. Gaussian components of the form

$$F_\lambda^G = F_0 \exp\left[-\frac{(\lambda-\lambda_c)^2}{2\sigma_G^2}\right] \quad (1)$$

are added to measure the emission and absorption features. The Gaussians are initially centered at the expected line center (λ_c), but are allowed to "float" in wavelength (λ), width (σ_G), and amplitude (F_0). The float in wavelength and width is required to compensate for wavelength calibration errors and the asymmetry of the broad emission lines. All Gaussian components without an initially fixed minimum width are constrained to have a minimum width of twice the instrumental profile (σ_G = 1.5 Å) to prevent fitting spurious pixels. Five separate regions containing emission and/or absorption features were examined separately, since slightly different procedures are needed to properly fit each spectral feature. These regions are: 1155 – 1315 Å

(Lyα and N V λ1240), 1307 - 1463 Å (C II λ1334, Si IV λ1398 and O IV] λ1402), 1425 - 1750 Å (N IV] λ1486, C IV λ1549, He II λ1640, and O III] λ1663), 1790 - 1960 Å (Al III λ1857, Si III] λ1890, and C III] λ1909), and 2640 - 2915 Å (Mg II λ2800).

To ensure an unbiased extraction of the parameters characterizing the UV emission and absorption features, the spectral components are systematically fit with a modified version of the MINUIT (James & Roos 1975) software. The CERN-developed MINUIT uses the non-linear least squares Levenberg-Marquart method to fit χ^2 minimizing Gaussian components to the spectral features. Errors in the fitting parameters are determined by exploring parameter space near the minimum and are reported as 1σ errors.

Complicated features such as C IV require multiple Gaussian components. While each new component will reduce χ^2, it may not always be statistically significant. In these cases, an F-test is applied (Bevington 1969). Only when the component passes the F-test will it be added to the final fit. As an additional restriction, we have chosen to limit the maximum number of components for each specific line (e.g., C IV λ1549) to three. All Gaussians were initially allowed a wide range of parameter space to achieve the best fit; this range was reduced as obvious trends of the fits became apparent.

Line fluxes were calculated by integrating and adding together the individual components of the feature of interest. A quadrature sum of the individual integrated Gaussian errors is not a true error estimate of the integrated flux, but in fact overestimates the true error. Similar to a method used in a previous campaign on NGC 5548 (Clavel et al. 1991), the point-to-point integrated light curve variations were used to scale the errors to the proper values.

Table 2 shows the allowed ranges and means of the final component fits. The components that were summed together to produce a measurement for a particular line or blend are described in the next subsection. Figure 2 shows an example of the combined fit to an individual SWP spectrum.

3.4 Summation of Line Components

We attach no physical significance to individual components for a particular line (e.g., C IV λ1549); the component fits are just a convenient description of the data. In addition, many of the individual emission and absorption lines in a given region are blended as a result of their proximity, and their individual light curves are noisy and difficult to interpret as a result of the fitting technique's inability to accurately deconvolve them. Therefore, as in the past (Clavel et al. 1991; Reichert et al. 1994), we use the sum of components to represent the dominant emission-line in a particular region. When we quote results for a particular sum of components, we use the dominant emission feature as a designation (e.g., "C IV" for the sum of the components of C IV and N IV]).

Many of the features in NGC 4151 are very difficult to measure accurately due to contamination and/or the complicated nature of the UV spectrum (many broad and narrow emission and absorption lines). Their light curves at relatively low levels of variability are very noisy, and cannot be used for the detailed analyses in Section 4. The redshift of NGC 4151 places its Lyα emission at 1219.7 Å, which is too close to the geocoronal emission to allow a separate fit to the two narrow components. Hence, the Lyα + N V light curve is dominated by the substantial variation of geocoronal Lyα over the course of each day, and is not usable for this study. As shown in Table 2, the Si IV + O IV] feature is dominated by a strong Si IV absorption doublet, and an accurate measurement of the intrsinic emission is not possible. Finally, the Mg II feature is strongly affected by the scattered light, particularly in the red wing.

The fluxes of the features around C IV, He II, and C III] can be measured accurately enough to produce reasonably good light curves. The C IV line profile is complicated, showing multicomponent emission and self-absorption. Due to their proximity, the C IV, N IV], He II, and O III] features are all fit simultaneously. The N IV], O III], and He II features are each fit with a single Gaussian, while the more complicated C IV feature is fit with three Gaussian components: a narrow emission component, a very narrow absorption component, and an extended emission component. The He II and O III] emission are blended, but distinct enough from the C IV emission, to be treated as a separate feature. Thus, we have separate measurments for C IV + N IV] and He II + O III].

The C III] region is modeled with an absorption component for Al III, a single emission component for Si III], and up to three emission components for C III], as shown in Table 2. Due to the asymmetry of the C III] emission, three components are needed: a narrow component, a broad component, and a component labeled "red". The red component is limited in central wavelength to avoid interference with the Si III] emission on the blue wing of C III]. The Al III absorption on the extreme blue wing of the emission can be separated from the overall feature, so the measurement is for C III] + Si III].

3.5 Comparison with IUESIPS

As a consistency check on the TOMSIPS processing scheme, we compared the measured continuum fluxes with those obtained in the same wavelength bins from the IUESIPS spectra. Figure 3 show this comparison for the 1275 Å bin, demonstrating that the fluxes from the two methods are extremely well correlated (the linear correlation coefficient is $r = 0.96$). The other SWP continuum bins show the same excellent correlation, with the TOMSIPS fluxes systematically higher than the IUESIPS fluxes by 1 – 10%, depending on the bin. This is a direct consequence of the slightly different (and improved) photometric correction and absolute sensitivity calibration as a function of wavelength.

4. Results

Tables 3 and 4 give the TOMSIPS continuum and line fluxes (and associated errors) as a function of Julian Date for the SWP and LWP spectra. The few observations that are not included in these tables are listed in section II.

4.1 Pattern of Variability

Figure 4 gives the SWP and LWP continuum light curves as a function of Julian Date. The light curves show significant variations on a number of different time scales, particularly at short wavelengths. The variations are as large as 40 – 50% on a time scale of several days, and ~10% on a time scale of several hours. During the 9.3 days of continuous monitoring, there were four large-amplitude "events" of duration 2 – 3 days (minimum to minimum). These events are temporally well resolved, and they are easily recognized in each continuum waveband. Many of the shorter time-scale, small-amplitude features also repeat in at least two different wavebands. The variations prior to and after the continuous monitoring period are clearly undersampled and are of limited use, although it is evident that there were strong variations during the last five days of the monitoring period.

Table 5 lists some basic properties of the variability in each waveband. The mean fluxes for the entire data set are given, as well as the mean errors, which are the average values of flux error divided by mean flux. F_{var}, the fractional variability, is the standard deviation of the fluxes divided by the mean flux in each waveband. It has been corrected to reflect the intrinsic variability by subtracting the mean error in quadrature. R_{max} is the ratio of largest to smallest mean flux in each waveband. It is clear from the parameters in Table 5 and from inspection of the light curves that there were significant variations in all continuum wavebands over this relatively short period of time. In particular, F_{var} is 4 – 10 times larger than the mean error, which is only about 1 – 1.5%.

The amplitude of the continuum variations decreases with increasing wavelength, as was the case for NGC 5548 (Clavel et al. 1989) and NGC 3783 (Reichert et al. 1994). This can be seen in both the F_{var} and R_{max} parameters. This result is in general agreement with previous IUE studies of NGC 4151 (e.g., Perola et al. 1982), which find that for larger amplitude (but undersampled) variations, the UV continuum radiation hardens as it brightens. The combination of the well-sampled UV variations described in this paper with those in the optical (Paper II) and X-ray regions (Paper III) permits a more detailed examination of the behavior of continuum amplitude as a function of wavelength (see Paper IV).

Figure 5 gives the light curves for the strongest lines in the SWP region. It is clear that the emission-line light curves are similar in appearance, with the fluxes rising through the first half of the campaign (over 8 – 9 days), and leveling off thereafter. C IV, the line with the smallest percentage errors, shows evidence for a subsequent shallow dip of duration ~3 days in its light curve before recovering to the previous maximum. The He II and C III] light curves appear to reflect these trends, although they are substantially noisier. There is a suggestion that the C III] and possibly the He II light curves reach the first maximum ~1 day before the C IV light curve. The reality of the shorter time-scale (~ 1 day) features in the emission-line light curves is uncertain, and it may be that the error bars for the He II and C III] points are underestimated.

The light curves of the emission-lines are substantially different in character compared to the continuum light curves. The continuum variations, which are very well defined, are much more rapid. Presumably, this is the result of a substantial response time of the lines to changes in the continuum, which will be explored in the next subsection.

Some basic properties of the emission-line variations are listed in Table 5. The fractional variability F_{var}, again corrected to reflect the intrinsic variability, and the ratio of largest to smallest flux R_{max} indicates that there were significant variations for all three emission lines shown. There is no obvious trend of larger variability amplitude for higher ionization lines, as was the case for NGC 5548 (Clavel et al. 1991) and NGC 3783 (Reichert et al. 1994), although we are restricted to only a few lines due to the small amplitude of variations over a short period of time and the complicated nature of the spectrum of NGC 4151. In light of previous studies, the larger amplitude of the He II variations is expected, but it is somewhat surpising that the amplitude of the C III] variations is larger than that of C IV.

4.2 Time-Series Analysis

Cross-correlation of a continuum light curve with a light curve from another continuum band, or an emission-line light curve, has been used in the past to determinine if the variations are correlated and if there is a time lag between the two series. Two distinct correlation functions were calculated for the UV light curves of NGC 4151: the interpolation cross-correlation function (CCF: cf. Gaskell & Sparke 1986; Gaskell & Peterson 1987) and the discrete correlation function (DCF: cf. Edelson & Krolik 1988). The correlations were calculated exactly in the manner described by White & Peterson (1994). The continuum light curve at 1275 Å was cross-correlated with that of each continuum bin and line feature, and in addition, the C IV light curve was cross-correlated with itself to generate its auto-correlation function (ACF). The calculations were performed for the subset of data obtained during the continuous monitoring period, and for all of the data obtained during the IUE campaign. The sampling interval chosen was 0.05 days (72 min), which is the approximate interval between consecutive observations with a particular camera during the continuous monitoring period.

Figures 6 and 7 show the continuum band CCF's and DCF's (which include error bars) for the continuous and entire data sets, respectively. For the continuous data, the CCF's and DCF's are nearly identical, as expected for regularly sampled light curves (White & Peterson 1994). The DCF is slightly higher in the 1 - 5 day range with the inclusion of the non-continuous data, whereas the CCF is significantly higher in this regime, where there is a significant amount of interpolation to a much finer grid for the days before and after the continuous monitoring period. Figures 8 and 9 show the emission-line CCF's and DCF's for the continuous and entire data sets, respectively. The regular sampling is again responsible for the agreement between CCF's and DCF's in Figure 8. In Figure 9, after a longer span of data is included, both CCF and DCF values are higher in the 1 - 5 day regime, and additional peaks in the correlation functions appear.

The most important conclusion to be drawn from these comparisons is that for the continuum bands, the CCF's and DCF's for both data sets give the same lag at which the peak correlation value occurs, to within ± 0.05 days. It is also clear from Figures 6 and 7 that the continuum variations are all highly correlated. For the emission-line features, the correlations with the continuum light curve at 1275 Å are much less significant. This is not a surprise, since the continuum and emission-line light curves are so different. As a result, the lags at which the peak values occur are not well defined and differ depending on type of correlation and data set used. However, the centroids of the data around peak values are similar for CCF's and DCF's from each data set.

Table 6 gives the main characteristics of the CCF's computed from the continuous monitoring of the continuum fluxes. The parameter Δt_{peak} gives the time lag (in days) for r_{max}, the peak value of the CCF, whereas $\Delta t_{centroid}$ gives the centroid in days for CCF values greater than $0.5 r_{max}$. The full width of the CCF at $0.5 r_{max}$ (FWHM) is also given. A negative value for Δt_{peak} or $\Delta t_{centroid}$ indicates that the variations for that feature precede those from the 1275 Å continuum bin.

Errors in the time lags were estimated using the analytic formula of Gaskell & Peterson (1987) and the Monte Carlo simulation method described by White & Peterson (1994). For the cross-correlation of the 1275 Å band with other UV continuum bands, both techniques yield 1 σ errors of 0.03 – 0.04 days. Given the slight differences in lags determined from different correlation techniques and different ways to measure the peak, a conservative estimate is that the lag errors are $\leq$ 0.10 days.

It is clear from Table 6 that the continuum variations in the various bands are all highly correlated, with r_{max} values in the range 0.70 – 0.92, and simultaneous to within $\pm$ 0.10 days (144 min), as evidenced by the small lags given by Δt_{peak} and $\Delta t_{centroid}$. The CCF for 2688 Å is somewhat unusual, with a secondary peak at $\sim$1.5 days. This could be the result of blended Fe II and/or Balmer continuum emission, which are often prominent in this wavelength region (Wills, Netzer, & Wills 1985) and likely vary on a longer time scale than the continuum, or it could be an indication of another continuum component. More careful modeling of the emission-lines in this region and/or detailed comparisons with the optical variations may help to distinguish between these possibilities. Nevertheless, it is evident that the prinicipal variations of the continuum at 2688 Å are synchronous with the variations at shorter wavelengths.

Figures 8 and 9 indicate that the emission-line variations are not well correlated with the continuum variations. In addition, the CCF's for the entire data set exhibit multiple peaks. This is a result of the fact that the continuum light curves show several quick events during the monitoring period, whereas the emission-line light curves show only one well-defined event of longer duration. The time scale for continuum changes in this instance appears to be substantially shorter than the response time of the emission-lines, as indicated by the large FWHM of the ACF for C IV (4.4 days) in the continuous data set compared to that of the 1275 Å continuum bin (1.2 days). Since the continuum and emission-line light curves are so dissimilar, the correlation functions are of limited use, and the lags at which the cross-correlations peak are not reported here. A more realistic value for the C IV emission-line lag has been determined with a data set of longer duration by Clavel et al. (1990).

5. Summary and Conclusions

We have observed the nucleus of NGC 4151 with IUE continuously for 9.3 days, obtaining a pair of SWP and LWP spectra every ~70 min, in the most intensive UV monitoring campaign to date for a Seyfert 1 galaxy. Observations were also obtained on the four days prior to and five days after the continuous monitoring period. The IUE observations are part of a multiwavelength effort to study the short time-scale (hours to days) variations of NGC 4151, which have not been well characterized in the past for any Seyfert 1 galaxy.

During the monitoring period, significant variations were detected in the fluxes of the continuum bands and the emission-line features. For the continuous monitoring period, there are four well-defined "events" in the UV continuum light curves, whereas the light curves for the strong emission lines are very different, showing only one major event (a slow rise followed by a shallow dip). Measurement and cross-correlation of the light curves allow us to draw some important conclusions:

1. The UV continuum of NGC 4151 can vary significantly on very short time scales, going through an "event" (i.e., a significant local maximum preceded and followed by local minima) in only 2 – 3 days. The amplitudes of the events in this case are small compared to those found in NGC 4151 over longer time scales (Clavel et al. 1990), but are large compared to the IUE errors, demonstrating the feasibility and importance of continuous monitoring of AGN in the UV.

2. The relative amplitudes of the continuum variations decrease with increasing wavelength, with R_{max} = 1.51, 1.45, 1.31, and 1.24 at λ = 1275 Å, 1440 Å, 1820 Å, and 2688 Å over the

monitoring period. This behavior has also been seen in the monitoring campaigns on NGC 5548 (Clavel et al. 1991; Korista et al. 1995) and NGC 3783 (Reichert et al. 1994) on longer time scales.

3. The continuum variations in all of the UV bands are *simultaneous* to within ±0.1 days (144 min). This is an important and very strict constraint compared to the upper limits on UV continuum lags obtained for NGC 5548 ($\Delta t_{peak} \lesssim 4$ days, Clavel et al. 1991; $\Delta t_{peak} \lesssim 1$ day, Korista et al. 1995) and NGC 3783 ($\Delta t_{peak} \lesssim 1$ days, Reichert et al. 1994).

4. The emission line variations of NGC 4151 are not always well correlated with the continuum variations over short periods of time (days or less). The apparent reason for the dissimilar continuum and emission-line light curves from our observations is the relatively short time scale for continuum variations compared to the response time of the emission-lines. Consequently, cross-correlations are not very useful tools in this case; better tools (e.g., techniques for determining the transfer function) and/or longer trains of data are required.

We are very grateful to the staff members of the Goddard and VILSPA IUE observatories for their assistance in scheduling and executing these demanding monitoring programs. We also wish to thank our many colleagues, including those on the IUE peer review committees, for their support of these programs. We gratefully acknowledge financial support of this particular program through NASA P.O. S-30917-F to Computer Sciences Corporation.

TABLE 1
LOG OF IUE OBSERVATIONS

Image Number	UT Date (Mon/Day/Yr)	UT Start (Hr:Min:Sec)	Duration (Min:Sec)	Julian Date (2,440,000+)	Exposure Levels (DN) Emis	Cont	Back	Notes
SWP 49333	11/27/93	07:52:24	21:00	9318.83535	202	160	15	
LWP 26815	11/27/93	08:27:10	11:00	9318.85602	180	160	31	
SWP 49334	11/27/93	08:59:41	19:00	9318.88138	187	95	15	
LWP 26816	11/27/93	09:34:43	13:00	9318.90362	200	180	33	
SWP 49335	11/27/93	10:03:40	20:00	9318.92616	200	95	19	
LWP 26817	11/27/93	10:35:00	13:00	9318.94549	195	188	33	
SWP 49341	11/28/93	07:22:27	20:00	9319.81420	193	100	20	
LWP 26822	11/28/93	07:58:10	14:00	9319.83692	254	200	33	
SWP 49342	11/28/93	08:27:54	20:00	9319.85965	192	110	20	
LWP 26823	11/28/93	09:00:59	12:00	9319.87985	220	190	33	
SWP 49343	11/28/93	09:35:26	21:00	9319.90690	200	110	20	
LWP 26824	11/28/93	10:10:22	12:00	9319.92803	230	190	35	
SWP 49362	11/29/93	08:01:53	20:00	9320.81159	198	100	20	
LWP 26831	11/29/93	08:37:10	12:00	9320.86331	219	190	35	
SWP 49363	11/29/93	09:08:14	20:00	9320.88766	200	95	19	
LWP 26832	11/29/93	09:43:00	15:00	9320.91007	239	210	33	
SWP 49364	11/29/93	10:13:36	20:00	9320.93306	205	105	20	
SWP 49372	11/30/93	07:49:04	20:00	9321.83269	205	137	15	
LWP 26836	11/30/93	08:25:56	14:00	9321.85620	243	180	33	
SWP 49373	11/30/93	08:57:37	21:00	9321.88064	232	109	14	
LWP 26837	11/30/93	09:31:53	14:00	9321.90200	248	183	34	
SWP 49374	11/30/93	10:02:20	21:00	9321.92558	214	113	15	
LWP 26838	11/30/93	10:35:13	12:00	9321.94529	218	189	35	
SWP 49379	12/01/93	03:26:32	20:00	9322.65037	191	113	16	
LWP 26846	12/01/93	04:07:01	12:00	9322.67571	227	178	36	1
SWP 49380	12/01/93	04:40:42	20:00	9322.70188	217	111	16	
LWP 26847	12/01/93	05:15:04	12:00	9322.72296	219	185	35	
SWP 49381	12/01/93	05:44:16	20:00	9322.74602	225	112	15	
LWP 26848	12/01/93	06:22:34	12:00	9322.76984	236	174	35	
SWP 49382	12/01/93	06:54:02	20:00	9322.79447	205	115	15	
LWP 26849	12/01/93	07:26:52	12:00	9322.81449	233	180	34	
SWP 49383	12/01/93	07:57:59	20:00	9322.83888	219	111	16	
LWP 26850	12/01/93	09:13:12	12:00	9322.88833	237	194	36	
SWP 49384	12/01/93	09:47:09	20:00	9322.91469	192	120	18	
LWP 26851	12/01/93	10:23:43	12:00	9322.93730	230	190	35	
SWP 49385	12/01/93	10:52:52	20:00	9322.96032	190	120	18	
LWP 26852	12/01/93	11:32:09	12:00	9322.98483	230	190	35	
SWP 49386	12/01/93	12:10:31	20:00	9323.01425	190	120	18	
LWP 26853	12/01/93	12:46:49	12:00	9323.03668	220	190	32	
SWP 49387	12/01/93	13:23:19	20:00	9323.06480	190	120	18	
LWP 26854	12/01/93	13:58:53	12:00	9323.08673	220	190	32	
SWP 49388	12/01/93	14:33:31	20:00	9323.11355	190	120	18	
LWP 26855	12/01/93	15:15:12	12:00	9323.13972	220	190	32	
SWP 49389	12/01/93	15:52:26	20:00	9323.16836	190	120	18	
LWP 26856	12/01/93	17:17:01	12:00	9323.22432	254	195	34	
SWP 49390	12/01/93	17:46:58	20:00	9323.24789	204	115	16	
LWP 26857	12/01/93	18:21:49	10:00	9323.26862	224	197	33	
SWP 49391	12/01/93	18:54:09	20:00	9323.29455	201	128	15	
LWP 26858	12/01/93	19:27:03	10:00	9323.31392	221	169	33	
SWP 49392	12/01/93	20:05:43	20:00	9323.34425	222	154	15	
LWP 26859	12/01/93	20:38:09	10:00	9323.36330	219	167	33	
SWP 49393	12/01/93	21:07:48	20:00	9323.38736	198	154	15	
LWP 26860	12/01/93	21:40:59	10:00	9323.40693	232	176	35	
SWP 49394	12/01/93	22:14:03	15:00	9323.43163	174	120	16	2
LWP 26861	12/02/93	01:10:08	10:00	9323.55218	215	147	33	
SWP 49395	12/02/93	01:41:56	20:00	9323.57773	196	108	15	
LWP 26862	12/02/93	02:17:40	10:00	9323.59907	212	160	34	
SWP 49396	12/02/93	02:53:33	20:00	9323.62747	195	113	15	
LWP 26863	12/02/93	03:29:33	10:00	9323.64899	206	163	33	
SWP 49397	12/02/93	04:06:15	20:00	9323.67795	205	113	16	

TABLE 1 *Continued*

Image Number	UT Date (Mon/Day/Yr)	UT Start (Hr:Min:Sec)	Duration (Min:Sec)	Julian Date (2,440,000+)	Exposure Levels (DN) Emis	Cont.	Back.	Notes
LWP 26864	12/02/93	04:41:27	10:00	9323.69892	217	164	33	
SWP 49398	12/02/93	05:17:21	20:00	9323.72733	228	119	17	
LWP 26865	12/02/93	05:53:10	10:00	9323.74875	215	163	34	
SWP 49399	12/02/93	06:29:06	20:00	9323.77715	217	119	16	
LWP 26866	12/02/93	07:03:07	10:00	9323.79730	217	166	34	
SWP 49400	12/02/93	07:32:56	20:00	9323.82148	216	116	16	
LWP 26867	12/02/93	08:09:07	10:00	9323.84314	215	166	33	
SWP 49401	12/02/93	09:14:33	20:00	9323.89205	207	131	12	
LWP 26868	12/02/93	09:49:01	12:00	9323.91321	240	163	23	
SWP 49402	12/02/93	10:19:05	20:00	9323.93686	205	130	12	
LWP 26869	12/02/93	10:54:55	12:00	9323.95897	240	160	23	
SWP 49403	12/02/93	11:26:00	20:00	9323.98333	205	130	12	
LWP 26870	12/02/93	12:05:03	12:00	9324.00767	240	160	23	
SWP 49404	12/02/93	12:43:51	20:00	9324.03740	205	130	12	
LWP 26871	12/02/93	13:18:53	12:00	9324.05895	240	160	23	
SWP 49405	12/02/93	13:56:50	20:00	9324.08808	205	130	12	
LWP 26872	12/02/93	14:43:16	12:00	9324.11755	240	160	23	
SWP 49406	12/02/93	15:16:01	20:00	9324.14307	205	130	12	
LWP 26873	12/02/93	15:54:05	12:00	9324.16673	240	160	23	
SWP 49407	12/02/93	16:25:43	20:00	9324.19147	232	141	17	
LWP 26874	12/02/93	17:27:24	10:00	9324.23083	218	188	35	
SWP 49408	12/02/93	17:52:27	20:00	9324.25170	214	134	15	
LWP 26875	12/02/93	18:25:18	10:00	9324.27104	220	193	35	1
SWP 49409	12/02/93	18:53:34	20:00	9324.29414	227	131	15	
LWP 26876	12/02/93	19:26:20	10:00	9324.31343	210	184	34	
SWP 49410	12/02/93	19:55:01	20:00	9324.33682	220	145	15	
LWP 26877	12/02/93	20:28:34	10:00	9324.35664	233	166	34	
SWP 49411	12/02/93	20:57:34	20:00	9324.38025	219	144	15	
LWP 26878	12/02/93	21:30:33	10:00	9324.39969	218	176	33	
SWP 49412	12/02/93	21:58:54	20:00	9324.42285	214	143	15	
LWP 26879	12/03/93	00:58:33	10:00	9324.54413	213	161	32	
SWP 49413	12/03/93	01:18:43	20:00	9324.56161	201	118	15	
LWP 26880	12/03/93	01:52:08	10:00	9324.58134	219	170	33	
SWP 49414	12/03/93	02:23:33	20:00	9324.60663	211	120	15	
LWP 26881	12/03/93	02:55:57	10:00	9324.62566	226	170	35	
SWP 49415	12/03/93	03:28:00	20:00	9324.65139	218	111	17	
LWP 26882	12/03/93	04:00:54	10:00	9324.67076	213	170	37	
SWP 49416	12/03/93	04:31:01	20:00	9324.69515	211	115	20	
LWP 26883	12/03/93	05:05:19	10:00	9324.71550	217	170	39	
SWP 49417	12/03/93	05:34:51	20:00	9324.73948	223	120	20	
LWP 26884	12/03/93	06:09:37	10:00	9324.76015	217	164	33	
SWP 49418	12/03/93	06:39:48	20:00	9324.78458	195	110	14	
LWP 26885	12/03/93	07:14:07	10:00	9324.80494	202	158	34	
SWP 49419	12/03/93	07:58:12	20:00	9324.83903	209	116	15	3
LWP 26886	12/03/93	08:54:54	12:00	9324.87563	239	170	23	
SWP 49420	12/03/93	09:20:32	20:00	9324.89620	223	116	16	
LWP 26887	12/03/93	09:57:00	12:00	9324.91875	240	170	23	
SWP 49421	12/03/93	10:27:27	20:00	9324.94267	270	115	16	
LWP 26888	12/03/93	11:04:08	12:00	9324.96537	240	170	23	
SWP 49422	12/03/93	11:34:14	20:00	9324.98905	220	115	16	
LWP 26889	12/03/93	12:06:11	12:00	9325.00846	240	170	23	
SWP 49423	12/03/93	12:47:47	20:00	9325.04013	220	115	16	
LWP 26890	12/03/93	13:27:03	12:00	9325.06462	240	170	23	
SWP 49424	12/03/93	13:57:50	20:00	9325.08877	208	110	16	
LWP 26891	12/03/93	14:30:38	12:00	9325.10877	240	170	23	
SWP 49425	12/03/93	15:06:07	20:00	9325.13619	208	110	16	
LWP 26892	12/03/93	15:40:43	12:00	9325.15744	240	170	23	
SWP 49426	12/03/93	16:11:40	20:00	9325.18171	208	110	16	
LWP 26893	12/03/93	17:25:31	12:00	9325.23022	242	177	37	
SWP 49427	12/03/93	17:49:33	20:00	9325.24969	218	121	24	

TABLE 1 - *Continued*

Image Number	UT Date (Mon/Day/Yr)	UT Start (Hr:Min:Sec)	Duration (Min:Sec)	Julian Date (2,440,000+)	Exposure Levels (DN) Ems.	Cont	Back	Notes
LWP 26894	12/03/93	18:27:26	10:00	9325.27245	220	168	35	4
SWP 49428	12/03/93	18:56:23	20:00	9325.29610	153	84	16	4
LWP 26895	12/03/93	19:29:57	10:00	9325.31591	167	130	31	4
SWP 49429	12/03/93	20:14:09	22:00	9325.35080	225	119	15	
LWP 26896	12/03/93	20:50:35	10:00	9325.37193	213	157	32	
SWP 49430	12/03/93	21:26:44	20:00	9325.40051	212	125	15	
LWP 26897	12/03/93	22:02:01	10:00	9325.42154	212	180	32	
SWP 49431	12/04/93	00:52:25	20:00	9325.54231	218	117	15	
LWP 26898	12/04/93	01:21:21	10:00	9325.55907	228	170	32	
SWP 49432	12/04/93	01:52:29	20:00	9325.58506	215	117	16	
LWP 26899	12/04/93	02:26:16	10:00	9325.60505	230	168	32	
SWP 49433	12/04/93	02:56:17	20:00	9325.62936	229	119	17	
LWP 26900	12/04/93	03:32:35	10:00	9325.65110	230	168	12	
SWP 49434	12/04/93	04:02:52	18:00	9325.67491	225	127	37	
LWP 26901	12/04/93	04:35:13	09:00	9325.69425	213	180	60	
SWP 49435	12/04/93	05:04:28	18:00	9325.71769	236	134	41	
LWP 26902	12/04/93	05:37:32	09:00	9325.73752	219	170	48	
SWP 49436	12/04/93	06:09:13	18:00	9325.76265	223	113	17	
LWP 26903	12/04/93	06:42:20	09:00	9325.78252	201	150	35	
SWP 49437	12/04/93	07:12:04	18:00	9325.80630	195	103	17	
LWP 26904	12/04/93	07:57:42	09:00	9325.83486	200	150	33	
SWP 49438	12/04/93	08:57:11	18:00	9325.87929	183	104	15	
LWP 26905	12/04/93	09:27:19	09:00	9325.89709	200	153	25	
SWP 49439	12/04/93	10:01:54	18:00	9325.92424	189	104	15	
LWP 26906	12/04/93	10:35:22	09:00	9325.94435	200	153	25	
SWP 49440	12/04/93	11:06:03	18:00	9325.96878	189	104	15	
LWP 26907	12/04/93	11:38:01	09:00	9325.98786	200	153	25	
SWP 49441	12/04/93	12:08:40	18:00	9326.01227	189	104	15	
LWP 26908	12/04/93	12:40:59	09:00	9326.03159	200	150	25	
SWP 49442	12/04/93	13:12:18	18:00	9326.05646	189	101	15	
LWP 26909	12/04/93	13:56:52	09:00	9326.08428	200	153	25	
SWP 49443	12/04/93	14:29:04	18:00	9326.10977	189	104	15	
LWP 26910	12/04/93	15:01:08	09:00	9326.12891	200	153	25	
SWP 49444	12/04/93	15:31:00	18:00	9326.15278	189	104	15	
LWP 26911	12/04/93	16:03:57	09:00	9326.17253	200	153	25	
SWP 49445	12/04/93	16:34:05	18:00	9326.19659	189	104	15	
LWP 26912	12/04/93	17:33:30	10:00	9326.23507	225	191	37	
SWP 49446	12/04/93	17:57:50	20:00	9326.25544	252	136	19	
LWP 26913	12/04/93	18:30:27	10:00	9326.27462	238	180	36	
SWP 49447	12/04/93	19:00:19	20:00	9326.29883	248	138	17	
LWP 26914	12/04/93	19:36:52	09:00	9326.32039	229	171	35	
SWP 49448	12/04/93	20:06:34	18:00	9326.34414	227	117	15	
LWP 26915	12/04/93	20:40:35	08:00	9326.36429	201	151	32	
SWP 49449	12/04/93	21:09:26	17:00	9326.38745	212	114	15	
LWP 26916	12/04/93	21:42:04	09:00	9326.40734	213	177	34	
SWP 49450	12/05/93	00:57:09	18:00	9326.54594	206	149	14	
LWP 26917	12/05/93	01:22:58	09:00	9326.56074	227	187	35	
SWP 49451	12/05/93	01:52:22	20:00	9326.58498	227	180	15	
LWP 26918	12/05/93	02:29:05	08:00	9326.60631	203	162	36	
SWP 49452	12/05/93	02:57:42	18:00	9326.62965	214	141	23	
LWP 26919	12/05/93	03:29:54	09:00	9326.64889	222	191	48	
SWP 49453	12/05/93	03:58:31	18:00	9326.67189	218	163	36	
LWP 26920	12/05/93	04:31:26	08:00	9326.69127	217	178	57	
SWP 49454	12/05/93	04:59:49	16:00	9326.71376	205	172	39	
LWP 26921	12/05/93	05:32:32	08:00	9326.73370	214	172	52	
SWP 49455	12/05/93	06:00:24	18:00	9326.75653	196	167	28	
LWP 26922	12/05/93	06:32:56	09:00	9326.77600	210	175	38	1
SWP 49456	12/05/93	07:02:48	20:00	9326.80056	208	146	16	
LWP 26923	12/05/93	07:35:00	09:00	9326.81910	210	182	33	
SWP 49457	12/05/93	08:18:27	20:00	9326.85309	234	160	15	

TABLE 1 *Continued*

Image Number	UT Date (Mon/Day/Yr)	UT Start (Hr:Min:Sec)	Duration (Min:Sec)	Julian Date (2,440,000+)	Exposure Levels (DN) Emis.	Cont.	Back.	Notes
LWP 26924	12/05/93	09:25:13	09:00	9326.89598	214	155	38	
SWP 49458	12/05/93	09:56:50	18:00	9326.92141	203	127	14	
LWP 26925	12/05/93	10:39:58	09:00	9326.94789	205	161	36	
SWP 49459	12/05/93	11:13:17	18:00	9326.97450	206	132	14	
LWP 26926	12/05/93	11:46:17	09:00	9326.99395	208	161	39	
SWP 49460	12/05/93	12:20:07	18:00	9327.02091	207	128	14	
LWP 26927	12/05/93	12:53:01	09:00	9327.04029	214	171	36	
SWP 49461	12/05/93	13:26:16	18:00	9327.06616	203	121	16	
LWP 26928	12/05/93	14:05:54	09:00	9327.09056	201	163	16	
SWP 49462	12/05/93	14:38:21	18:00	9327.11621	202	121	16	
LWP 26929	12/05/93	15:13:31	09:00	9327.13751	201	163	16	
SWP 49463	12/05/93	15:46:30	18:00	9327.16354	202	121	16	
LWP 26930	12/05/93	16:29:59	09:00	9327.19061	201	163	16	
SWP 49464	12/05/93	17:15:18	18:00	9327.22521	248	120	16	
LWP 26931	12/05/93	17:44:15	09:00	9327.24219				5
SWP 49465	12/05/93	18:19:24	16:30	9327.26903	219	110	15	
LWP 26932	12/05/93	18:59:09	09:00	9327.29420				
SWP 49466	12/05/93	19:32:32	17:00	9327.32016	242	115	15	
LWP 26933	12/05/93	20:03:57	09:00	9327.33920	236	174	35	
SWP 49467	12/05/93	20:49:38	16:00	9327.37336	194	104	14	
LWP 26934	12/05/93	21:21:45	8:00	9327.39288	205	161	33	
SWP 49468	12/05/93	21:52:14	17:00	9327.41718	227	110	15	
SWP 49470	12/06/93	00:41:47	16:30	9327.53457	198	140	14	
LWP 26935	12/06/93	01:06:42	08:30	9327.54910	210	164	35	
SWP 49471	12/06/93	01:36:12	17:00	9327.57271	216	132	15	
LWP 26936	12/06/93	02:15:29	09:00	9327.59721	218	179	36	
SWP 49472	12/06/93	02:44:03	17:00	9327.61983	204	130	21	
LWP 26937	12/06/93	03:16:57	09:00	9327.63990	233	182	46	
SWP 49473	12/06/93	03:47:21	18:00	9327.66413	215	148	38	
LWP 26938	12/06/93	04:18:54	07:00	9327.68222	193	161	56	
SWP 49474	12/06/93	04:48:10	17:00	9327.70602	229	154	47	
LWP 26939	12/06/93	05:23:14	09:00	9327.72759	222	184	58	
SWP 49475	12/06/93	05:52:24	18:00	9327.75097	243	139	27	
LWP 26940	12/06/93	06:24:42	10:00	9327.77062	224	187	38	
SWP 49476	12/06/93	06:53:05	20:00	9327.79381	192	131	16	
LWP 26941	12/06/93	07:25:25	10:00	9327.81279	215	176	35	
SWP 49477	12/06/93	07:59:54	20:00	9327.84021	209	125	15	
LWP 26942	12/06/93	08:58:34	10:00	9327.87748	214	155	38	
SWP 49478	12/06/93	09:24:08	20:00	9327.89870	203	127	14	
LWP 26943	12/06/93	09:58:49	10:00	9327.91932	205	161	36	1
SWP 49479	12/06/93	10:28:32	20:00	9327.94343	206	132	14	
LWP 26944	12/06/93	11:06:05	10:00	9327.96603	208	161	39	
SWP 49480	12/06/93	11:36:00	20:00	9327.99028	207	128	14	
LWP 26945	12/06/93	12:08:34	10:00	9328.00942	214	171	36	
SWP 49481	12/06/93	12:37:37	20:00	9328.03307	215	132	16	
LWP 26946	12/06/93	13:24:20	10:00	9328.06204	222	171	34	
SWP 49482	12/06/93	13:54:32	20:00	9328.08648	205	140	16	
LWP 26947	12/06/93	14:27:32	10:00	9328.10593	224	164	36	
SWP 49483	12/06/93	14:55:24	20:00	9328.12875	201	128	17	
LWP 26948	12/06/93	15:27:34	10:00	9328.14762	222	182	37	
SWP 49484	12/06/93	16:00:48	20:00	9328.17417	209	134	21	
LWP 26949	12/06/93	16:49:00	10:00	9328.20417	233	182	38	
SWP 49485	12/06/93	17:14:37	20:00	9328.22543	228	123	17	
LWP 26950	12/06/93	17:49:53	10:00	9328.24645	230	164	36	
SWP 49486	12/06/93	18:23:43	20:00	9328.27341	249	127	17	
LWP 26951	12/06/93	18:57:58	10:00	9328.29373	233	171	37	
SWP 49487	12/06/93	19:28:24	18:00	9328.31764	204	110	15	
LWP 26952	12/06/93	20:00:37	09:00	9328.33689	223	161	35	
SWP 49488	12/06/93	20:34:47	18:00	9328.36374	213	115	15	
LWP 26953	12/06/93	21:07:07	09:00	9328.38307	216	150	35	

TABLE 1 - *Continued*

Image Number	UT Date (Mon/Day/Yr)	UT Start (Hr:Min:Sec)	Duration (Min:Sec)	Julian Date (2.440,000+)	Exposure Levels (DN) Emis.	Cont.	Back.	Notes
SWP 49489	12/06/93	21:37:09	18:00	9328.40705	188	107	15	
SWP 49491	12/07/93	00:49:48	19:00	9328.54118	189	122	14	
LWP 26954	12/07/93	01:16:10	09:00	9328.55602	203	164	34	
SWP 49492	12/07/93	01:46:15	21:00	9328.58108	202	136	16	
LWP 26955	12/07/93	02:17:48	10:00	9328.59917	223	182	36	
SWP 49493	12/07/93	02:46:25	22:00	9328.62321	209	149	26	
LWP 26956	12/07/93	03:19:56	10:00	9328.64231	224	187	50	
SWP 49494	12/07/93	03:48:08	22:00	9328.66607	233	165	42	
LWP 26957	12/07/93	04:20:23	09:00	9328.68395	207	184	59	
SWP 49495	12/07/93	04:49:06	20:00	9328.70771	210	154	45	
LWP 26958	12/07/93	05:21:30	09:00	9328.72639	206	187	59	
SWP 49496	12/07/93	05:49:52	21:00	9328.75026	211	146	31	
LWP 26959	12/07/93	06:22:21	10:00	9328.76899	207	181	41	
SWP 49497	12/07/93	06:51:00	22:00	9328.79306	205	137	16	
LWP 26960	12/07/93	07:23:10	10:00	9328.81123	205	173	35	
SWP 49498	12/07/93	07:58:49	22:00	9328.84015	237	144	16	
LWP 26961	12/07/93	08:52:45	11:00	9328.87379	221	169	37	
SWP 49499	12/07/93	09:16:22	20:00	9328.89331	225	136	18	
LWP 26962	12/07/93	09:49:40	10:00	9328.91296	209	163	37	
SWP 49500	12/07/93	10:18:53	20:00	9328.93672	211	141	17	
LWP 26963	12/07/93	10:50:15	10:00	9328.95503	207	162	37	
SWP 49501	12/07/93	11:25:21	20:00	9328.98288	195	139	17	
LWP 26964	12/07/93	11:57:03	10:00	9329.00142	232	184	35	
SWP 49502	12/07/93	12:30:42	20:00	9329.02826	200	136	18	
LWP 26965	12/07/93	13:04:18	10:00	9329.04812	230	175	39	
SWP 49503	12/07/93	13:33:08	20:00	9329.07162	211	119	18	
LWP 26966	12/07/93	14:04:16	10:00	9329.08977	221	174	38	
SWP 49504	12/07/93	14:32:59	20:00	9329.11318	196	133	15	
LWP 26967	12/07/93	15:04:35	10:00	9329.13165	218	166	36	
SWP 49505	12/07/93	15:36:14	20:00	9329.15711	232	157	17	
LWP 26968	12/07/93	16:11:39	10:00	9329.17823	223	175	34	
SWP 49506	12/07/93	16:58:11	20:00	9329.21402	215	112	20	6
LWP 26969	12/07/93	17:27:09	09:00	9329.23031	229	168	35	
SWP 49507	12/07/93	17:56:42	19:00	9329.25430	217	112	21	
LWP 26970	12/07/93	18:32:48	09:00	9329.27590	221	167	37	
SWP 49508	12/07/93	19:04:54	19:00	9329.30167	210	129	18	
LWP 26971	12/07/93	19:39:00	09:00	9329.32187	211	168	35	
SWP 49509	12/07/93	20:09:02	19:00	9329.34620	206	124	17	
LWP 26972	12/07/93	20:43:00	09:00	9329.36632	206	167	35	
SWP 49510	12/07/93	21:14:34	20:00	9329.39206	213	117	18	6
LWP 26973	12/07/93	21:48:47	09:00	9329.41200	213	166	36	
SWP 49511	12/07/93	22:21:16	20:00	9329.43838	200	126	18	6
SWP 49512	12/08/93	00:35:57	20:00	9329.53191	221	131	15	
LWP 26974	12/08/93	01:04:27	10:00	9329.54823	217	177	34	
SWP 49513	12/08/93	01:33:46	19:00	9329.57171	214	133	15	
LWP 26975	12/08/93	02:06:13	10:00	9329.59112	222	185	34	
SWP 49514	12/08/93	02:34:04	19:00	9329.61359	213	131	15	
LWP 26976	12/08/93	03:07:17	10:00	9329.63353	217	185	36	
SWP 49515	12/08/93	03:34:39	20:00	9329.65601	220	148	15	
LWP 26977	12/08/93	04:07:40	10:00	9329.67546	207	176	35	1
SWP 49516	12/08/93	04:35:52	19:00	9329.69817	211	140	17	
LWP 26978	12/08/93	05:10:48	10:00	9329.71931	228	176	36	
SWP 49517	12/08/93	05:38:44	19:00	9329.74183	216	132	15	
LWP 26979	12/08/93	06:10:17	10:00	9329.76061	210	180	35	
SWP 49518	12/08/93	06:39:15	19:00	9329.78385	198	136	15	
LWP 26980	12/08/93	07:11:39	10:00	9329.80323	208	173	35	
SWP 49519	12/08/93	07:49:13	20:00	9329.83279	213	122	15	
LWP 26981	12/08/93	08:38:24	10:00	9329.86347	211	165	34	
SWP 49520	12/08/93	09:05:15	20:00	9329.88559	214	135	17	
LWP 26982	12/08/93	09:39:33	10:00	9329.90594	222	166	34	

TABLE 1 - *Continued*

Image Number	UT Date (Mon/Day/Yr)	UT Start (Hr:Min:Sec)	Duration (Min:Sec)	Julian Date (2,440,000+)	Exposure Levels (DN) Emis.	Cont.	Back.	Notes
SWP 49521	12/08/93	10:08:55	20:00	9329.92980	225	133	16	
LWP 26983	12/08/93	10:41:07	10:00	9329.94869	216	168	35	1
SWP 49522	12/08/93	11:16:14	20:00	9329.97655	218	130	16	
LWP 26984	12/08/93	11:52:55	10:00	9329.99855	222	163	34	1
SWP 49523	12/08/93	12:22:05	20:00	9330.02228	214	145	17	
LWP 26985	12/08/93	13:03:16	10:00	9330.04741	208	160	36	1
SWP 49524	12/08/93	13:37:25	20:00	9330.07459	208	122	17	
LWP 26986	12/08/93	14:08:36	10:00	9330.09278	210	169	35	
SWP 49525	12/08/93	14:37:37	20:00	9330.11640	233	139	17	
LWP 26987	12/08/93	15:08:54	10:00	9330.13465	215	176	36	
SWP 49526	12/08/93	15:40:03	20:00	9330.15976	224	139	18	
LWP 26988	12/08/93	16:11:04	10:00	9330.17782	221	173	37	
SWP 49527	12/08/93	16:54:10	20:00	9330.21123	232	122	21	
LWP 26989	12/08/93	17:23:20	10:00	9330.22801	236	194	37	1
SWP 49528	12/08/93	17:52:31	20:00	9330.25175	229	130	18	
LWP 26990	12/08/93	18:29:24	10:00	9330.27389	229	182	35	
SWP 49529	12/08/93	18:58:20	20:00	9330.29745	229	162	18	
LWP 26991	12/08/93	19:34:21	10:00	9330.31899	238	179	34	1
SWP 49530	12/08/93	20:08:01	20:00	9330.34584	237	123	18	
LWP 26992	12/08/93	20:43:49	10:00	9330.36723	232	178	36	
SWP 49531	12/08/93	21:10:52	18:00	9330.38880	194	108	16	
LWP 26993	12/08/93	21:46:46	10:00	9330.41095	220	163	36	
SWP 49533	12/09/93	00:31:59	19:00	9330.52881	218	120	15	
LWP 26994	12/09/93	00:58:23	10:00	9330.54402	222	190	33	
SWP 49534	12/09/93	01:27:21	19:00	9330.56726	211	120	15	
LWP 26995	12/09/93	02:02:51	10:00	9330.58879	224	192	33	
SWP 49535	12/09/93	02:32:21	19:00	9330.61240	213	120	15	
LWP 26996	12/09/93	03:06:05	10:00	9330.63270	230	186	35	
SWP 49536	12/09/93	03:35:38	19:00	9330.65634	210	120	18	
LWP 26997	12/09/93	04:14:14	09:00	9330.67968	208	177	39	
SWP 49537	12/09/93	04:43:01	19:00	9330.70314	202	115	20	
LWP 26998	12/09/93	05:16:29	09:00	9330.72290	206	160	38	
SWP 49538	12/09/93	05:45:08	19:00	9330.74627	194	125	15	
LWP 26999	12/09/93	06:18:33	09:00	9330.76601	210	173	34	
SWP 49539	12/09/93	06:47:53	20:00	9330.79020	189	120	16	
LWP 27000	12/09/93	07:25:32	09:30	9330.81252	201	154	35	
SWP 49540	12/09/93	08:05:19	20:00	9330.84397	221	124	15	
LWP 27001	12/09/93	09:08:41	09:30	9330.88416	208	153	38	
SWP 49541	12/09/93	09:39:26	20:00	9330.90933	203	112	18	
LWP 27002	12/09/93	10:21:03	09:30	9330.93441	210	160	38	
SWP 49542	12/09/93	10:57:44	20:00	9330.96370	202	110	19	
LWP 27003	12/09/93	11:32:57	09:30	9330.98434	209	154	39	
SWP 49543	12/09/93	12:02:09	20:00	9331.00844	203	118	19	
LWP 27004	12/09/93	12:38:19	09:30	9331.02973	209	171	38	
SWP 49544	12/09/93	13:16:05	20:00	9331.05978	192	120	18	
LWP 27005	12/09/93	13:52:40	09:30	9331.08137	217	168	37	
SWP 49545	12/09/93	14:25:37	20:00	9331.10807	202	92	20	
LWP 27006	12/09/93	15:03:25	09:30	9331.13050	208	166	37	
SWP 49546	12/09/93	15:32:36	20:00	9331.15458	197	162	19	
LWP 27007	12/09/93	16:11:17	09:30	9331.17763	213	165	37	
SWP 49547	12/09/93	16:56:54	21:30	9331.21347	227	133	16	
LWP 27008	12/09/93	17:27:58	10:00	9331.23123				5
SWP 49548	12/09/93	17:56:41	21:00	9331.25499	227	130	20	
LWP 27009	12/09/93	18:31:42	10:00	9331.27549	245	168	36	
SWP 49549	12/09/93	19:01:40	21:00	9331.30012	226	141	20	
LWP 27010	12/09/93	19:38:06	09:00	9331.32125	239	168	36	
SWP 49550	12/09/93	20:08:02	20:00	9331.34586	227	113	19	
SWP 49551	12/09/93	21:05:29	20:00	9331.38575	226	127	20	
LWP 27012	12/09/93	21:41:18	09:00	9331.40681	220	167	35	
SWP 49553	12/10/93	00:17:15	19:00	9331.51858	204	117	15	

TABLE 1 - *Continued*

Image Number	UT Date (Mon/Day/Yr)	UT Start (Hr:Min:Sec)	Duration (Min:Sec)	Julian Date (2,440,000+)	Exposure Levels (DN) Emis.	Cont.	Back	Notes
LWP 27013	12/10/93	00:44:14	09:00	9331.53384	213	150	32	
SWP 49554	12/10/93	01:14:37	20:00	9331.55876	225	120	15	
LWP 27014	12/10/93	01:50:15	10:00	9331.58003	232	167	32	
SWP 49555	12/10/93	02:19:19	20:00	9331.60369	212	120	15	
LWP 27015	12/10/93	02:54:11	10:00	9331.62443	227	165	38	
SWP 49556	12/10/93	03:23:42	20:00	9331.64840	235	150	25	
LWP 27016	12/10/93	03:58:05	10:00	9331.66881	227	155	43	
SWP 49557	12/10/93	04:27:56	19:00	9331.69266	219	136	24	
LWP 27017	12/10/93	05:04:01	10:00	9331.71460	241	161	44	
SWP 49558	12/10/93	05:33:43	19:00	9331.73834	220	125	20	
SWP 49559	12/10/93	07:09:07	18:00	9331.80425	206	115	15	
LWP 27019	12/10/93	07:43:56	09:0	9331.82530	208	150	35	
SWP 49560	12/10/93	08:18:41	18:00	9331.85256	186	109	15	
SWP 49567	12/11/93	05:57:11	19:00	9332.75464	198	120	15	
LWP 27024	12/11/93	06:50:15	10:00	9332.78837	217	155	37	7
SWP 49568	12/11/93	07:07:29	20:00	9332.80381	222	115	15	
LWP 27025	12/11/93	07:42:12	10:30	9332.82444	218	155	35	
SWP 49569	12/11/93	08:15:30	20:00	9332.85104	211	129	15	
SWP 49574	12/12/93	05:35:33	21:00	9333.74031	185	120	18	
LWP 27030	12/12/93	06:06:12	11:00	9333.75813	198	155	36	
SWP 49575	12/12/93	06:35:57	24:00	9333.78330	210	120	15	
LWP 27031	12/12/93	07:10:41	13:00	9333.80360	223	163	36	
SWP 49576	12/12/93	07:40:26	25:30	9333.82843	235	140	15	
LWP 27032	12/12/93	08:15:09	13:30	9333.84837	240	158	37	
SWP 49582	12/13/93	05:50:03	24:00	9334.75142	233	126	15	
LWP 27034	12/13/93	06:18:55	13:00	9334.76765	251	167	34	
SWP 49583	12/13/93	06:49:05	22:30	9334.79173	210	124	15	
LWP 27035	12/13/93	07:20:59	11:30	9334.81006	221	160	34	
SWP 49584	12/13/93	07:50:15	23:00	9334.83455	212	118	15	
LWP 27036	12/13/93	08:23:53	12:00	9334.85408	209	164	35	
SWP 49592	12/14/93	05:42:29	24:00	9335.74617	228	139	16	
LWP 27040	12/14/93	06:09:47	13:00	9335.76131	251	196	34	
SWP 49593	12/14/93	06:40:28	23:00	9335.78609	214	122	15	
LWP 27041	12/14/93	07:14:19	11:30	9335.80543	219	173	34	
SWP 49594	12/14/93	07:43:58	23:00	9335.83018	233	124	14	
LWP 27042	12/14/93	08:17:06	12:00	9335.84938	228	178	34	
SWP 49600	12/15/93	05:49:46	22:00	9336.75053	208	136	14	
LWP 27048	12/15/93	06:18:25	12:00	9336.76696	249	186	34	
SWP 49601	12/15/93	06:46:47	24:00	9336.79082	225	137	15	
SWP 49602	12/15/93	07:39:30	23:00	9336.82708	240	144	15	
LWP 27050	12/15/93	08:22:12	11:00	9336.85257	235	191	34	

Notes:

1. Microphonics present.
2. Noisy. Exposure cut short due to Earth occultation.
3. Header incorrectly says image number is SWP 49418.
4. Pointing error. Target on edge of aperture.
5. Lost most of image due to telemetry problems.
6. Lyα slightly overexposed
7. Exposed for additional 10 min in high dispersion.

TABLE 2

GAUSSIAN COMPONENTS RANGES, MEANS, AND STANDARD DEVIATIONS

Fitted Component	F_G (10^{-11} ergs s^{-1} cm^{-2} $Å^{-1}$) Min	Mean	Max	λ_c (Å) Min	Mean	Max	σ_G (Å) Min	Mean	Max
Lyα - Absorption	-212.9	112.0± 30.6	-51.5	1211.0	1215.5± 1.9	1220.0	1.8	4.4± 1.3	8.0
Lyα - Narrow	95.2	164.0± 29.5	270.0	1212.8	1217.5± 1.3	1220.2	2.1	3.4± 0.4	4.5
Lyα - Broad	39.6	87.6± 19.6	172.5	1216.1	1219.9± 1.3	1222.0	8.7	12.6± 1.5	15.5
N V	-60.0	-41.1± 8.8	-20.1	1236.0	1238.1± 1.0	1240.0	2.6	3.9± 0.4	5.0
C II - Absorption	-14.7	-9.3± 2.1	-5.5	1327.0	1330.7± 1.3	1333.6	1.5	2.9± 0.7	5.0
Si IV - Absorption 1	-32.5	-23.5± 3.8	-11.2	1387.0	1389.5± 0.9	1392.0	1.7	3.1± 0.6	4.1
Si IV - Absorption 2	-23.9	-15.7± 3.0	-5.8	1396.0	1398.4± 0.8	1401.0	1.3	2.1± 0.3	3.0
Si IV + O IV] - Emission	6.0	12.6± 3.9	17.5	1388.0	1390.3± 1.8	1395.5	6.0	12.0± 2.6	16.0
N IV]	2.0	6.2± 1.9	11.5	1480.0	1486.1± 3.1	1491.0	0.7	6.6± 2.5	9.0
C IV - Absorption	-110.0	-89.6± 8.8	-70.0	1543.0	1544.9± 0.9	1547.0	2.7	3.3± 0.2	4.0
C IV - Narrow	62.8	78.2± 7.7	99.6	1544.0	1545.8± 0.8	1547.7	7.5	9.7± 1.1	12.0
C IV - Broad	23.8	38.7± 3.8	50.5	1543.0	1546.1± 1.6	1551.0	27.5	34.5± 2.1	36.5
He II	16.0	19.8± 1.9	25.7	1636.0	1638.1± 1.0	1640.0	4.5	8.4± 1.7	10.5
O III]	7.0	10.8± 1.5	14.5	1657.4	1662.8± 2.0	1666.0	4.5	8.9± 1.0	9.5
Al III Absorption	-5.0	-2.6± 1.0	0.0	1848.0	1854.1± 3.3	1860.0	0.0	4.6± 1.9	8.0
Si III]	4.0	7.3± 1.7	10.5	1879.0	1884.2± 2.8	1890.0	3.9	9.9± 1.2	10.5
C III] - Narrow	13.9	21.0± 3.0	28.3	1901.0	1903.4± 1.0	1905.8	3.3	4.9± 0.5	6.1
C III] - Broad	3.0	6.6± 2.8	12.0	1903.0	1907.3± 4.7	1919.0	7.0	13.3± 3.0	17.0
C III] - RED	1.0	3.8± 1.5	8.0	1912.0	1915.0± 1.1	1918.0	0.7	2.5± 0.9	4.7

TABLE 3

SWP FLUXES[a]

Julian Date (2,440,000+)	F_λ(1275 A)	F_λ(1440 A)	F_λ(1820 A)	F(C IV)	F(He II)	F(C III])
9318.83535	36.94±0.34	33.77±0.51	25.67±0.34	19.25±0.29	2.21±0.11	2.69±0.10
9318.88138	35.88±0.37	32.69±0.54	25.74±0.36	19.59±0.29	2.45±0.11	2.65±0.10
9318.92616	36.63±0.36	32.25±0.52	25.01±0.35	19.81±0.27	2.50±0.11	2.65±0.10
9319.81420	36.27±0.35	33.17±0.52	26.05±0.36	19.92±0.29	2.34±0.11	2.84±0.10
9319.85965	38.64±0.37	34.15±0.53	26.84±0.36	19.68±0.29	2.25±0.11	2.86±0.10
9319.90690	38.45±0.36	34.43±0.51	26.42±0.33	19.63±0.29	2.35±0.11	2.79±0.10
9320.84159	37.98±0.37	34.53±0.53	27.91±0.35	19.38±0.29	2.64±0.11	2.79±0.10
9320.88766	38.74±0.37	36.22±0.54	27.30±0.35	19.58±0.27	2.92±0.11	2.90±0.10
9320.93306	38.50±0.36	35.37±0.53	27.29±0.36	19.74±0.29	2.85±0.11	2.98±0.10
9321.83269	37.33±0.36	33.52±0.52	27.03±0.36	19.96±0.15	2.69±0.11	2.85±0.10
9321.88064	38.89±0.36	34.12±0.51	27.00±0.34	20.36±0.29	2.62±0.11	2.77±0.10
9321.92558	38.96±0.36	35.14±0.52	28.04±0.36	20.66±0.29	2.75±0.11	2.75±0.10
9322.65037	40.47±0.37	36.60±0.54	27.52±0.35	21.23±0.15	2.76±0.11	2.79±0.11
9322.70188	40.82±0.38	35.48±0.54	27.12±0.35	21.30±0.29	2.81±0.11	2.81±0.10
9322.74602	39.94±0.38	36.52±0.54	28.53±0.37	21.00±0.27	2.94±0.11	2.89±0.10
9322.79447	40.78±0.38	37.10±0.54	29.16±0.36	21.20±0.29	3.08±0.11	2.91±0.10
9322.83888	43.33±0.39	37.15±0.54	28.81±0.35	21.40±0.29	3.13±0.11	2.78±0.11
9322.91469	44.40±0.40	37.95±0.56	29.30±0.37	21.58±0.29	3.03±0.11	2.76±0.10
9322.96032	44.46±0.40	38.17±0.55	28.89±0.37	21.48±0.27	3.07±0.11	2.76±0.10
9323.01425	44.62±0.40	37.26±0.54	28.65±0.37	21.40±0.29	3.10±0.11	2.94±0.11
9323.06480	44.77±0.40	38.53±0.55	29.28±0.37	21.63±0.27	3.15±0.11	3.00±0.11
9323.11355	44.19±0.40	37.95±0.54	28.96±0.37	21.29±0.29	3.10±0.11	2.85±0.10
9323.16836	44.75±0.40	38.15±0.55	30.17±0.36	21.06±0.29	3.03±0.11	2.96±0.10
9323.24789	42.06±0.38	38.80±0.55	28.29±0.36	20.70±0.29	2.97±0.11	2.97±0.10
9323.29455	42.95±0.38	39.81±0.55	29.06±0.35	20.98±0.27	2.97±0.11	3.01±0.10
9323.34425	44.26±0.39	37.46±0.54	29.02±0.35	21.13±0.29	3.09±0.11	2.81±0.10
9323.38736	43.13±0.39	37.70±0.55	29.19±0.36	21.52±0.15	3.19±0.12	2.84±0.10
9323.57773	42.90±0.39	37.13±0.55	28.82±0.35	21.53±0.29	3.21±0.11	2.81±0.10
9323.62746	42.76±0.39	36.19±0.53	29.21±0.35	21.80±0.29	3.10±0.11	2.86±0.10
9323.67795	45.04±0.39	37.76±0.55	29.03±0.36	21.93±0.29	2.86±0.11	2.89±0.10
9323.72733	43.03±0.39	37.63±0.55	29.49±0.37	21.90±0.29	2.73±0.11	2.89±0.10
9323.77715	44.87±0.40	38.05±0.54	30.72±0.36	22.04±0.29	2.87±0.11	2.98±0.10
9323.82148	44.56±0.39	38.83±0.55	29.58±0.36	22.37±0.27	3.01±0.11	2.84±0.10
9323.89205	43.17±0.38	36.52±0.54	29.14±0.35	22.47±0.29	3.20±0.11	2.78±0.10
9323.93686	42.46±0.39	37.87±0.55	29.62±0.36	22.19±0.15	3.28±0.11	2.74±0.10
9323.98333	42.72±0.39	38.53±0.56	28.99±0.37	21.68±0.27	3.14±0.11	2.91±0.10
9324.03740	42.48±0.39	37.01±0.54	28.95±0.37	21.78±0.29	3.17±0.11	3.13±0.10
9324.08808	43.58±0.40	37.51±0.54	29.28±0.37	22.05±0.29	3.03±0.11	3.13±0.10
9324.14307	44.02±0.40	36.08±0.54	27.86±0.37	21.99±0.29	3.29±0.11	2.97±0.10
9324.19147	42.49±0.40	36.71±0.55	28.64±0.38	21.81±0.29	3.25±0.11	2.94±0.10
9324.25170	43.40±0.39	37.95±0.54	28.67±0.35	21.29±0.29	3.42±0.11	2.81±0.10
9324.29414	43.87±0.40	37.74±0.54	28.98±0.36	21.50±0.27	3.35±0.11	2.93±0.10
9324.33682	42.18±0.39	37.40±0.54	27.94±0.37	21.63±0.29	3.28±0.11	3.01±0.10
9324.38025	40.80±0.38	38.20±0.55	28.60±0.37	21.84±0.29	3.22±0.11	3.09±0.11
9324.42285	40.96±0.38	36.84±0.54	28.82±0.36	21.80±0.29	3.05±0.11	3.01±0.10
9324.56161	40.54±0.38	37.55±0.53	28.47±0.35	21.75±0.29	2.89±0.11	2.94±0.10
9324.60663	40.99±0.38	36.94±0.53	28.32±0.36	21.41±0.27	2.93±0.11	2.94±0.10
9324.65139	42.83±0.39	38.18±0.55	27.92±0.36	21.74±0.29	3.07±0.11	2.96±0.10
9324.69515	40.93±0.39	36.25±0.56	27.91±0.37	21.93±0.29	3.28±0.11	2.89±0.10
9324.73948	40.84±0.39	36.54±0.55	28.00±0.38	22.47±0.29	3.25±0.11	2.91±0.10
9324.78458	40.18±0.38	35.57±0.53	28.06±0.35	21.78±0.29	3.19±0.11	2.95±0.11
9324.83903	40.05±0.37	37.25±0.54	28.23±0.35	21.96±0.29	3.17±0.11	3.07±0.10
9324.89620	38.89±0.37	35.22±0.53	28.41±0.35	22.16±0.29	3.10±0.11	3.18±0.10
9324.94267	40.48±0.38	34.97±0.53	27.98±0.35	22.36±0.29	3.25±0.11	3.39±0.10
9324.98905	39.73±0.38	35.68±0.53	27.22±0.35	22.19±0.29	3.06±0.11	3.26±0.10
9325.04013	38.47±0.36	34.92±0.53	27.95±0.37	22.03±0.29	2.85±0.11	3.02±0.10
9325.08877	38.85±0.37	35.57±0.54	27.35±0.35	22.15±0.29	2.90±0.11	2.69±0.11
9325.13619	39.25±0.37	35.18±0.53	27.83±0.36	22.06±0.29	3.23±0.11	3.00±0.10

TABLE 3 – *Continued*

Julian Date (2,440,000+)	F_λ(1275 Å)	F_λ(1440 Å)	F_λ(1820 Å)	F(C IV)	F(He II)	F(C III])
9325.18171	40.78±0.39	35.55±0.54	27.22±0.36	21.86±0.29	3.26±0.11	3.13±0.10
9325.24969	38.40±0.38	36.69±0.55	28.28±0.37	22.05±0.29	3.14±0.11	3.38±0.10
9325.35080	39.54±0.36	36.11±0.51	28.09±0.35	22.01±0.27	2.99±0.11	3.14±0.10
9325.40051	40.56±0.37	37.03±0.54	28.54±0.37	22.39±0.27	3.05±0.11	3.15±0.10
9325.54334	40.26±0.38	38.19±0.54	29.18±0.36	22.38±0.27	3.05±0.11	3.12±0.10
9325.58506	43.89±0.39	39.03±0.55	29.38±0.37	22.59±0.29	3.29±0.11	3.20±0.10
9325.62936	44.22±0.40	39.37±0.56	29.18±0.37	23.02±0.29	3.55±0.11	3.21±0.11
9325.67491	44.49±0.47	39.89±0.69	29.14±0.47	22.89±0.29	3.68±0.11	3.17±0.10
9325.71769	46.26±0.51	39.38±0.72	30.02±0.51	22.92±0.29	3.61±0.11	3.12±0.11
9325.76265	46.18±0.44	39.56±0.60	29.99±0.42	22.10±0.29	3.68±0.11	3.14±0.10
9325.80630	45.30±0.44	40.89±0.61	29.07±0.40	22.46±0.29	3.57±0.11	3.10±0.11
9325.87929	43.74±0.42	38.75±0.58	30.03±0.38	22.28±0.29	3.61±0.11	3.11±0.10
9325.92424	45.82±0.42	38.96±0.58	30.02±0.39	22.43±0.29	3.44±0.11	3.10±0.10
9325.96878	46.67±0.42	39.78±0.59	30.29±0.39	22.40±0.29	3.40±0.11	3.23±0.10
9326.01227	45.57±0.42	39.34±0.59	30.09±0.40	22.86±0.29	3.19±0.11	3.43±0.10
9326.05646	47.47±0.43	38.45±0.59	29.17±0.40	22.93±0.27	3.14±0.11	3.48±0.11
9326.10977	46.90±0.43	40.38±0.60	30.65±0.40	22.60±0.29	3.05±0.11	3.50±0.10
9326.15278	48.47±0.45	42.31±0.62	30.24±0.40	22.62±0.29	3.29±0.11	3.28±0.11
9326.19659	49.80±0.45	41.71±0.61	32.03±0.42	23.23±0.27	3.26±0.11	3.33±0.10
9326.25544	50.09±0.44	42.74±0.60	32.27±0.41	23.47±0.29	3.36±0.11	3.37±0.10
9326.29883	50.15±0.43	43.76±0.59	32.46±0.39	23.13±0.29	3.40±0.11	3.56±0.10
9326.34414	49.78±0.44	42.86±0.61	31.66±0.41	22.55±0.29	3.59±0.11	3.52±0.10
9326.38745	51.45±0.46	43.07±0.63	32.51±0.41	22.89±0.29	3.57±0.11	3.56±0.10
9326.54594	51.54±0.45	41.72±0.60	32.27±0.40	22.79±0.29	3.60±0.11	3.45±0.10
9326.58498	51.92±0.43	43.35±0.57	31.62±0.38	23.47±0.29	3.70±0.11	3.52±0.10
9326.62965	51.47±0.48	44.34±0.65	32.71±0.45	23.24±0.29	3.78±0.11	3.60±0.11
9326.67189	52.30±0.52	44.99±0.73	32.64±0.51	23.86±0.29	3.60±0.11	3.94±0.10
9326.71376	53.92±0.58	44.25±0.80	32.78±0.57	23.69±0.29	3.50±0.11	3.91±0.11
9326.75653	54.34±0.50	44.79±0.68	32.78±0.46	23.89±0.29	3.55±0.11	3.85±0.10
9326.80056	52.24±0.44	43.07±0.57	31.38±0.39	23.57±0.29	3.63±0.11	3.61±0.10
9326.85309	52.83±0.44	43.80±0.57	31.92±0.37	23.38±0.29	3.58±0.11	3.57±0.11
9326.92141	52.52±0.46	43.02±0.62	30.89±0.39	23.09±0.29	3.52±0.11	3.62±0.10
9326.97450	51.37±0.45	44.24±0.62	31.01±0.41	23.44±0.29	3.36±0.11	3.58±0.11
9327.02091	51.17±0.44	42.85±0.61	31.63±0.39	23.39±0.29	3.32±0.11	3.53±0.10
9327.06616	51.00±0.44	43.26±0.61	31.33±0.38	23.84±0.29	3.34±0.11	3.45±0.10
9327.11621	51.17±0.45	43.05±0.61	30.88±0.41	23.97±0.27	3.50±0.11	3.57±0.10
9327.16354	49.42±0.44	41.89±0.61	30.63±0.39	23.75±0.29	3.57±0.11	3.66±0.11
9327.22521	51.86±0.46	44.27±0.62	31.99±0.42	23.76±0.29	3.69±0.11	3.58±0.10
9327.26920	51.15±0.48	40.48±0.63	31.94±0.42	23.54±0.29	3.66±0.11	3.43±0.10
9327.32016	49.79±0.46	41.82±0.63	31.77±0.42	24.04±0.29	3.81±0.11	3.37±0.11
9327.37336	49.57±0.47	40.09±0.63	30.33±0.42	23.99±0.15	3.63±0.11	3.40±0.10
9327.41718	48.81±0.44	40.46±0.62	30.55±0.40	23.55±0.27	3.61±0.11	3.42±0.11
9327.53474	47.47±0.44	39.41±0.62	29.22±0.40	23.28±0.29	3.34±0.11	3.47±0.11
9327.57271	47.10±0.44	39.23±0.60	29.87±0.40	23.36±0.29	3.35±0.11	3.35±0.10
9327.61983	47.01±0.46	39.15±0.63	30.42±0.44	23.48±0.29	3.28±0.11	3.37±0.10
9327.66413	47.94±0.50	41.75±0.73	29.56±0.51	24.05±0.15	3.52±0.11	3.52±0.11
9327.70602	48.37±0.55	40.86±0.79	29.61±0.55	24.40±0.29	3.44±0.11	3.58±0.10
9327.75097	47.19±0.47	40.05±0.65	30.05±0.46	24.59±0.29	3.65±0.11	3.62±0.10
9327.79381	45.03±0.40	38.57±0.55	30.33±0.37	24.13±0.29	3.47±0.11	3.48±0.10
9327.84021	43.71±0.39	39.64±0.55	29.18±0.36	23.69±0.27	3.62±0.11	3.36±0.10
9327.89870	43.53±0.39	36.42±0.54	28.92±0.39	24.01±0.29	3.50±0.11	3.35±0.10
9327.94343	44.60±0.40	35.76±0.53	29.03±0.37	24.41±0.29	3.40±0.11	3.29±0.10
9327.99028	44.04±0.39	36.03±0.53	29.09±0.36	24.59±0.27	3.35±0.11	3.47±0.10
9328.03307	43.47±0.39	36.94±0.54	28.37±0.36	24.28±0.29	3.32±0.11	3.34±0.10
9328.08648	43.17±0.38	37.14±0.55	28.97±0.37	24.41±0.29	3.48±0.11	3.32±0.10
9328.12875	43.58±0.39	36.71±0.54	28.49±0.36	24.30±0.29	3.55±0.11	3.30±0.11
9328.17417	44.02±0.41	37.57±0.56	29.56±0.38	24.28±0.29	3.61±0.11	3.25±0.10
9328.22543	44.13±0.40	39.36±0.57	29.17±0.37	23.96±0.27	3.42±0.11	3.39±0.10

TABLE 3 - *Continued*

Julian Date (2,440,000+)	F_λ(1275 Å)	F_λ(1440 Å)	F_λ(1820 Å)	F(C IV)	F(He II)	F(C III])
9328.27341	45.21±0.43	37.89±0.55	28.36±0.37	24.15±0.27	3.49±0.11	3.35±0.11
9328.31764	44.23±0.42	36.73±0.58	29.20±0.39	24.18±0.29	3.42±0.11	3.39±0.10
9328.36371	43.37±0.41	36.78±0.57	28.65±0.39	24.58±0.29	3.56±0.11	3.21±0.10
9328.40705	42.54±0.41	36.43±0.57	28.37±0.39	23.98±0.29	3.38±0.11	3.11±0.10
9328.54118	41.44±0.39	36.09±0.55	28.39±0.36	23.70±0.29	3.29±0.11	3.13±0.10
9328.58108	42.24±0.38	37.51±0.53	29.15±0.35	23.43±0.29	3.31±0.11	3.09±0.10
9328.62321	44.05±0.40	39.17±0.56	28.60±0.37	23.20±0.29	3.11±0.11	3.27±0.10
9328.66607	44.99±0.45	40.74±0.64	26.70±0.42	23.26±0.29	3.11±0.11	3.39±0.10
9328.70771	44.55±0.49	39.58±0.70	28.54±0.47	23.58±0.15	2.86±0.12	3.64±0.10
9328.75026	45.09±0.43	39.34±0.61	28.59±0.41	23.97±0.29	3.17±0.11	3.60±0.11
9328.79306	44.29±0.38	39.06±0.52	28.89±0.35	23.75±0.27	3.32±0.11	3.47±0.11
9328.84015	44.15±0.37	38.77±0.52	29.33±0.34	23.50±0.29	3.42±0.11	3.36±0.11
9328.89331	45.56±0.40	38.92±0.55	29.35±0.36	24.15±0.29	3.34±0.11	3.31±0.10
9328.93673	44.60±0.40	38.40±0.56	29.54±0.38	24.43±0.29	3.27±0.11	3.31±0.10
9328.98288	46.95±0.41	37.86±0.55	29.53±0.37	24.44±0.29	3.51±0.11	3.42±0.10
9329.02826	46.42±0.41	39.13±0.55	30.19±0.38	24.26±0.29	3.65±0.11	3.50±0.10
9329.07162	46.76±0.41	40.09±0.56	29.47±0.38	24.03±0.27	3.64±0.11	3.41±0.10
9329.11318	48.05±0.42	40.57±0.57	31.07±0.38	24.08±0.29	3.47±0.11	3.21±0.10
9329.15711	48.60±0.42	39.76±0.56	30.79±0.37	23.77±0.29	3.49±0.11	3.11±0.10
9329.21402	48.63±0.42	39.20±0.55	30.49±0.37	24.02±0.29	3.65±0.11	3.26±0.10
9329.25431	46.39±0.41	40.41±0.58	29.67±0.37	24.01±0.29	3.79±0.11	3.35±0.10
9329.30167	47.39±0.42	39.23±0.57	31.00±0.38	24.27±0.29	3.62±0.11	3.43±0.11
9329.34620	48.32±0.43	38.12±0.57	30.42±0.39	23.64±0.29	3.48±0.11	3.30±0.10
9329.39206	46.53±0.40	38.39±0.54	30.24±0.36	23.46±0.29	3.31±0.11	3.33±0.10
9329.43838	45.96±0.38	37.24±0.52	29.37±0.38	22.92±0.29	3.54±0.11	3.32±0.10
9329.53191	43.49±0.40	37.42±0.54	28.62±0.35	23.56±0.29	3.60±0.11	3.41±0.10
9329.57171	42.53±0.40	38.08±0.56	28.90±0.38	23.69±0.29	3.71±0.11	3.40±0.10
9329.61359	41.83±0.39	36.20±0.55	28.13±0.37	23.86±0.15	3.49±0.11	3.57±0.11
9329.65601	42.03±0.38	36.54±0.53	27.52±0.35	23.56±0.29	3.28±0.11	3.55±0.10
9329.69817	41.61±0.40	37.08±0.57	28.47±0.39	23.46±0.27	3.29±0.11	3.49±0.10
9329.74183	41.36±0.39	35.82±0.56	28.15±0.36	23.84±0.29	3.33±0.11	3.44±0.10
9329.78385	41.00±0.39	35.42±0.55	27.98±0.37	24.14±0.29	3.39±0.11	3.49±0.10
9329.83279	39.59±0.37	35.42±0.53	26.35±0.35	23.86±0.29	3.33±0.11	3.53±0.11
9329.88559	39.88±0.38	35.86±0.53	27.86±0.35	23.27±0.15	3.29±0.11	3.37±0.10
9329.92980	39.54±0.37	35.97±0.53	27.71±0.36	22.79±0.29	3.36±0.11	3.36±0.10
9329.97655	40.39±0.37	35.03±0.53	26.92±0.36	23.15±0.29	3.35±0.11	3.32±0.10
9330.02228	41.22±0.38	35.18±0.54	27.46±0.35	22.87±0.29	3.33±0.11	3.18±0.11
9330.07459	39.21±0.38	35.99±0.53	27.65±0.35	23.36±0.29	3.25±0.11	3.09±0.10
9330.11640	40.12±0.37	34.36±0.53	27.99±0.37	23.30±0.29	3.15±0.11	3.12±0.10
9330.15976	39.59±0.38	35.34±0.53	28.89±0.36	23.64±0.29	3.23±0.11	3.32±0.10
9330.21123	40.55±0.39	35.67±0.54	27.06±0.35	23.31±0.29	3.16±0.11	3.34±0.10
9330.25175	39.23±0.37	37.48±0.55	28.43±0.36	23.25±0.29	3.23±0.11	3.28±0.11
9330.29745	40.00±0.37	36.35±0.54	27.69±0.36	23.50±0.27	3.13±0.11	3.38±0.10
9330.34584	41.40±0.39	36.12±0.53	27.55±0.35	23.56±0.29	3.12±0.11	3.46±0.10
9330.38880	40.99±0.39	35.30±0.56	27.70±0.38	23.69±0.29	3.06±0.11	3.51±0.10
9330.52881	40.17±0.37	36.27±0.54	27.31±0.36	23.84±0.29	2.95±0.11	3.38±0.10
9330.56726	40.60±0.39	36.10±0.55	27.63±0.36	23.59±0.27	3.07±0.11	3.28±0.10
9330.61240	40.62±0.39	36.28±0.54	28.20±0.36	23.50±0.29	3.12±0.11	3.30±0.10
9330.65634	41.61±0.40	36.11±0.57	27.25±0.39	23.53±0.27	3.21±0.11	3.14±0.10
9330.70314	42.72±0.42	35.75±0.57	28.00±0.39	24.03±0.29	3.32±0.11	3.23±0.10
9330.74627	41.34±0.40	35.37±0.56	28.47±0.38	24.03±0.27	3.35±0.11	3.34±0.10
9330.79020	41.48±0.38	36.60±0.54	27.40±0.35	23.80±0.15	3.29±0.11	3.57±0.10
9330.84397	43.04±0.40	36.15±0.54	27.59±0.36	23.99±0.27	3.21±0.11	3.57±0.11
9330.90933	42.04±0.39	36.29±0.54	28.65±0.37	23.48±0.29	3.29±0.11	3.36±0.10
9330.96370	43.17±0.39	37.70±0.55	28.87±0.35	23.53±0.29	3.26±0.11	3.42±0.10
9331.00844	43.52±0.40	36.20±0.54	27.81±0.36	23.50±0.15	3.16±0.11	3.44±0.10
9331.05978	43.31±0.39	35.28±0.53	28.02±0.37	24.07±0.29	3.25±0.11	3.58±0.10
9331.10807	43.32±0.40	36.43±0.54	28.72±0.37	23.82±0.29	3.38±0.11	3.39±0.10

TABLE 3 — *Continued*

Julian Date (2,440,000+)	F_λ(1275 Å)	F_λ(1440 Å)	F_λ(1820 Å)	F(C IV)	F(He II)	F(C III])
9331.15158	43.62±0.40	36.61±0.54	27.57±0.35	22.83±0.27	3.29±0.11	3.33±0.10
9331.21365	43.33±0.39	39.14±0.53	28.89±0.36	23.21±0.29	3.09±0.11	3.32±0.11
9331.25499	42.40±0.38	36.51±0.53	28.49±0.36	23.74±0.27	3.11±0.11	3.52±0.10
9331.30012	42.43±0.39	37.21±0.53	28.07±0.36	24.87±0.29	3.31±0.11	3.43±0.10
9331.34586	42.94±0.38	35.37±0.52	28.85±0.38	24.69±0.29	3.29±0.11	3.40±0.10
9331.38575	42.06±0.38	36.13±0.54	27.58±0.34	23.96±0.29	3.46±0.11	3.19±0.10
9331.51858	39.24±0.38	35.27±0.54	26.32±0.36	23.57±0.29	3.51±0.11	3.23±0.11
9331.55876	38.16±0.36	35.14±0.54	27.21±0.36	23.25±0.27	3.66±0.11	3.25±0.10
9331.60369	40.15±0.38	35.14±0.53	27.78±0.36	23.53±0.29	3.50±0.11	3.46±0.11
9331.64840	39.85±0.40	36.62±0.57	27.02±0.37	23.90±0.29	3.55±0.11	3.67±0.11
9331.69266	39.22±0.40	35.56±0.59	27.18±0.41	23.92±0.15	3.51±0.11	3.80±0.10
9331.73834	37.72±0.39	33.90±0.55	26.24±0.38	24.26±0.15	3.45±0.11	3.69±0.10
9331.80425	36.86±0.39	32.47±0.55	26.44±0.36	24.07±0.29	3.16±0.11	3.53±0.10
9331.85256	37.09±0.37	30.99±0.53	25.94±0.36	24.06±0.29	3.09±0.11	3.31±0.10
9332.75464	42.61±0.38	36.73±0.55	27.48±0.35	24.44±0.15	3.25±0.11	3.28±0.10
9332.80381	41.76±0.38	36.39±0.54	29.26±0.36	24.30±0.27	3.53±0.11	3.44±0.11
9332.85104	42.67±0.39	36.40±0.54	28.21±0.35	24.33±0.27	3.58±0.11	3.37±0.10
9333.74031	38.47±0.36	33.57±0.52	27.45±0.37	23.90±0.29	3.54±0.11	3.36±0.10
9333.78330	38.26±0.33	34.03±0.47	26.67±0.31	24.10±0.27	3.47±0.11	3.27±0.10
9333.82860	38.13±0.32	33.49±0.45	26.55±0.30	24.58±0.29	3.42±0.11	3.37±0.10
9334.75142	37.84±0.34	32.84±0.46	26.27±0.31	24.56±0.29	3.35±0.11	3.33±0.10
9334.79190	37.45±0.35	32.91±0.49	26.46±0.32	24.13±0.27	3.24±0.11	3.27±0.10
9334.83455	38.30±0.35	35.54±0.49	26.37±0.31	23.60±0.15	3.28±0.12	3.41±0.10
9335.74617	42.78±0.36	36.36±0.49	27.49±0.33	23.29±0.29	3.26±0.11	3.43±0.10
9335.78609	42.27±0.36	36.11±0.49	28.79±0.34	23.75±0.29	3.23±0.11	3.50±0.10
9335.83018	41.66±0.36	36.89±0.49	27.81±0.33	24.29±0.29	3.30±0.11	3.31±0.10
9336.75053	44.35±0.37	37.02±0.50	29.86±0.34	24.99±0.29	3.39±0.11	3.26±0.10
9336.79082	42.41±0.35	35.61±0.48	28.08±0.32	25.28±0.27	3.58±0.11	3.28±0.10
9336.82708	44.31±0.37	36.54±0.50	28.63±0.33	25.53±0.27	3.61±0.11	3.55±0.10

[a] Rest-frame continuum fluxes in units of 10^{-14} ergs s^{-1} cm^{-2} $Å^{-1}$.
Rest-frame line fluxes in units of 10^{-12} ergs s^{-1} cm^{-2}.

TABLE 4

IWE FLUXES[a]

Julian Date (2,440,000+)	F_λ(2688 Å)	Julian Date (2,440,000+)	F_λ(2688 Å)	Julian Date (2,440,000+)	F_λ(2688 Å)	Julian Date (2,440,000+)	F_λ(2688 Å)
9318.85602	17.92±0.20	9324.71550	18.87±0.23	9327.49288	20.78±0.25	9329.90593	19.77±0.23
9318.90362	17.75±0.18	9324.76015	18.99±0.22	9327.54927	20.56±0.24	9329.91866	19.05±0.22
9318.94549	17.92±0.18	9324.80494	18.58±0.21	9327.59721	20.56±0.24	9329.99855	18.75±0.21
9319.83692	17.83±0.18	9324.87563	19.21±0.20	9327.63990	20.95±0.26	9330.04741	19.24±0.22
9319.87985	17.82±0.19	9324.91875	18.95±0.20	9327.68222	21.57±0.33	9330.09278	18.88±0.21
9319.92803	17.41±0.19	9324.96537	18.89±0.20	9327.72759	21.12±0.29	9330.13467	19.05±0.22
9320.86331	18.00±0.19	9325.00846	19.25±0.20	9327.77062	20.38±0.23	9330.17782	19.12±0.22
9320.91007	18.12±0.17	9325.06462	19.07±0.20	9327.81279	20.38±0.22	9330.22801	19.56±0.22
9321.85620	18.00±0.18	9325.10877	18.85±0.20	9327.87748	20.40±0.22	9330.27389	19.55±0.22
9321.90200	18.39±0.18	9325.15744	18.82±0.20	9327.91932	20.83±0.22	9330.31898	19.72±0.22
9321.94529	18.17±0.19	9325.23022	19.15±0.20	9327.96603	20.37±0.22	9330.36723	20.14±0.22
9322.67571	18.48±0.20	9325.37193	19.27±0.22	9328.00642	20.35±0.22	9330.41095	19.88±0.22
9322.72296	18.77±0.20	9325.42154	19.44±0.22	9328.06204	20.54±0.22	9330.54402	19.61±0.22
9322.76984	18.76±0.20	9325.55997	19.00±0.22	9328.10593	20.60±0.22	9330.58879	19.44±0.22
9322.81449	18.84±0.20	9325.60505	19.20±0.22	9328.14762	20.28±0.23	9330.63270	20.07±0.22
9322.88833	19.36±0.20	9325.65110	19.74±0.24	9328.20417	20.33±0.23	9330.67968	20.87±0.24
9322.93730	19.15±0.20	9325.69425	20.04±0.28	9328.24645	20.45±0.23	9330.72290	21.65±0.25
9322.98483	19.17±0.20	9325.73752	20.67±0.27	9328.29373	20.66±0.23	9330.76601	21.46±0.24
9323.03668	19.29±0.20	9325.78252	19.54±0.23	9328.33689	20.66±0.24	9330.81270	20.24±0.23
9323.08673	19.09±0.20	9325.83486	18.98±0.23	9328.38307	20.18±0.23	9330.88433	19.04±0.22
9323.13972	19.27±0.20	9325.89709	19.79±0.23	9328.55602	19.67±0.23	9330.93458	20.11±0.23
9323.22432	19.86±0.20	9325.94435	19.88±0.23	9328.59917	21.06±0.23	9330.98451	20.02±0.22
9323.26862	19.31±0.22	9325.98786	19.92±0.23	9328.64231	20.77±0.25	9331.02991	20.42±0.23
9323.31392	19.39±0.22	9326.03159	20.25±0.23	9328.68395	20.87±0.28	9331.08154	20.12±0.23
9323.36330	19.46±0.22	9326.08428	19.72±0.24	9328.72639	21.36±0.29	9331.13067	20.50±0.23
9323.40693	19.40±0.22	9326.12891	19.86±0.24	9328.76899	20.26±0.23	9331.17780	20.30±0.23
9323.55218	19.16±0.22	9326.17253	20.16±0.24	9328.81123	20.22±0.22	9331.27549	19.88±0.22
9323.59907	19.22±0.22	9326.23507	20.59±0.23	9328.87379	20.70±0.21	9331.32127	[illegible]
9323.64899	19.38±0.22	9326.27462	20.25±0.23	9328.91296	20.56±0.22	9331.40681	[illegible]
9323.69892	19.49±0.22	9326.32039	20.51±0.24	9328.95503	20.49±0.22	9331.53384	19.29±0.22
9323.74873	19.41±0.22	9326.36429	20.43±0.25	9329.00142	20.84±0.23	9331.58003	19.50±0.22
9323.79730	19.60±0.22	9326.40734	20.76±0.24	9329.04812	21.26±0.23	9331.62443	19.72±0.22
9323.84314	19.78±0.22	9326.56074	20.82±0.24	9329.08977	20.84±0.23	9331.66881	20.02±0.23
9323.91324	19.18±0.20	9326.60631	20.66±0.25	9329.13165	21.19±0.23	9331.71460	19.90±0.24
9323.95897	19.28±0.20	9326.64889	20.82±0.26	9329.17823	20.97±0.23	9331.82530	19.44±0.23
9324.00767	19.42±0.20	9326.69127	21.29±0.30	9329.23031	20.88±0.24	9332.78837	20.31±0.22
9324.05895	19.18±0.20	9326.73370	20.86±0.30	9329.27590	20.92±0.24	9332.82462	20.56±0.22
9324.11755	18.95±0.20	9326.77600	21.01±0.25	9329.32187	21.00±0.24	9333.75813	19.64±0.21
9324.16673	19.18±0.20	9326.81910	20.64±0.24	9329.36632	20.68±0.24	9333.80360	19.82±0.19
9324.23083	19.14±0.22	9326.89598	21.07±0.24	9329.41200	20.13±0.23	9333.84854	19.84±0.19
9324.27104	19.35±0.22	9326.94789	20.74±0.23	9329.54823	20.50±0.22	9334.76765	19.72±0.19
9324.31343	19.40±0.22	9326.99395	20.83±0.24	9329.59112	20.43±0.22	9334.81023	19.95±0.21
9324.35664	19.45±0.22	9327.04029	20.95±0.24	9329.63353	20.07±0.22	9334.85409	19.29±0.20
9324.39969	19.31±0.22	9327.09056	21.08±0.24	9329.67546	19.43±0.22	9335.76131	19.98±0.19
9324.54413	18.53±0.21	9327.13751	20.84±0.24	9329.71931	19.46±0.22	9335.80500	20.07±0.21
9324.58134	18.88±0.21	9327.19061	21.04±0.25	9329.76061	19.53±0.22	9335.84938	20.29±0.20
9324.62566	19.51±0.22	9327.29420	20.97±0.24	9329.80323	19.43±0.22	9336.76696	20.01±0.20
9324.67076	18.79±0.22	9327.33920	21.20±0.24	9329.86347	19.19±0.22	9336.85257	20.08±0.21

[a]Rest-frame continuum fluxes in units of 10^{-14} ergs s^{-1} cm^{-2} $Å^{-1}$.

TABLE 5

VARIABILITY PARAMETERS

Feature	Mean Flux[a]	Mean Error	F_{var}	R_{max}
F_{λ}(1275 Å)	43.45	0.009	0.091	1.51
F_{λ}(1440 Å)	37.66	0.015	0.076	1.45
F_{λ}(1820 Å)	28.83	0.013	0.052	1.31
F_{λ}(2688 Å)	19.83	0.011	0.042	1.24
F(C IV)	22.98	0.012	0.054	1.33
F(He II)	3.27	0.033	0.082	1.70
F(C III])	3.25	0.030	0.078	1.49

[a]Continuum fluxes in units of 10^{-14} ergs s^{-1} cm^{-2} Å^{-1}.
Line fluxes in units of 10^{-12} ergs s^{-1} cm^{-2}.

TABLE 6

CONTINUUM CROSS-CORRELATION RESULTS

Feature[a]	Δt_{peak} (days)	$\Delta t_{centroid}$ (days)	r_{max}	FWHM (days)
1275 Å (ACF)	0.00	0.00	1.00	1.20
1440 Å	−0.05	−0.08	0.92	1.31
1820 Å	−0.05	−0.08	0.91	1.26
2688 Å	0.00	0.10	0.70	1.26

[a] Correlated against the light curve at 1275 Å.

REFERENCES

Ayres, T. 1993, PASP, 105, 538

Bevington, P. R. 1969, Data Reduction and Error Analysis for the Physical Sciences, 200

Bromage, G.E., et al. 1985, MNRAS, 215, 1

Carini, M., & Weinstein, D. 1992, NASA IUE Newsletter, [illegible], 5

Clavel, J. et al. 1987, ApJ, 321, 251

Clavel, J., et al. 1990, MNRAS, 246, 668

Clavel, J., et al. 1991, ApJ, 366, 64

Clavel, J. et al. 1992, ApJ, 393, 113

Collin-Souffrin, S. 1991, A&A, 249, 344

Courvoisier, T.J.-L. & Clavel, J. 1991, A&A, 248, 349

Dietrich, M., et al. 1993, ApJ, 408, 416

Edelson, R.A., & Krolik, J.H. 1988, ApJ, 333, 646

Edelson, R.A., et al. 1995, ApJ, 438, 120.

Edelson, R.A., et al. 1995b, in preparation (Paper IV)

Evans, I.N., et al. 1993, ApJ, 417, 82

Gaskell, C.M., & Peterson, B.M., 1987, ApJS, 65, 1

Gaskell, C.M., & Sparke, L.S. 1986, ApJ, 305, 175

Holt, S.S., et al. 1980, ApJ, 241, L13

James, F., & Roos M. 1975, Computer Physics Communications, 10, 343

Johnston, K.J., Elvis, M., Kjer, D., & Shen, B.S.P. 1982, ApJ, 262, 61

Kaspi, S., et al. 1995, in preparation (paper II)

Kinney, A.L., Bohlin, R.C., & Neill, J.D. 1991 PASP, 103, 694

Korista, K.T., et al. 1995, ApJ, in press

Kriss, G. A., et al. 1992, ApJ, 392, 485

Krolik, J.H., et al. 1991, ApJ, 371, 541

Maoz, D., et al. 1991, ApJ, 367, 493

Newmark, J.S., et al. 1992, NASA IUE Newsletter, 47, 1

Osterbrock, D.E. & Koski, A.T. 1976, MNRAS, 176, 61P

Penston, M.V., et al. 1981, MNRAS, 196, 857

Penton, S.V., et al. 1995, in preparation

Perola, G.C., et al. 1982, MNRAS 200, 293

Peterson, B.M., 1993, PASP, 105, 247

Peterson, B.M., et al. 1991, ApJ, 368, 119

Peterson, B.M., et al. 1992, ApJ, 392, 470

Peterson, B.M., et al. 1994, ApJ, 425, 622

Reichert, G.A., et al. 1994, ApJ, 425, 582

Shakura, R.I. & Sunyaev, R.A. 1973, A&A, 24, 337

Simkin, S.M. 1975, ApJ, 200, 567

Stirpe, G.M., et al. 1994, ApJ, 425, 609

Ulrich, M.-H., et al. 1985, Nature, 313, 745

Ulrich, M.-H., et al. 1991, ApJ, 382, 483

Warwick, R.S., et al. 1995, in preparation (paper III)

Weaver, K. A., et al. 1994a, ApJ, 423, 621
Weaver, K., Yaqoob, T., Holt, S. S., Mushotzky, R. F., Matsuoka, M., & Yamauchi, M. 1994b, ApJ, 436, L27
White, R.J., & Peterson, B.M. 1994, ApJ, 106, 879
Wilson, A.S., & Ulvestad, J.S. 1982, ApJ 263, 576
Yaqoob, T., Warwick, R., & Pounds, K. 1989, MNRAS, 236, 153

FIGURE CAPTIONS

FIG. 1- Averaged and combined SWP and LWP spectrum of NGC 4151 for the 1993 campaign. The 1975 - 2500 Å region has been smoothed with a 10 pixel (~15 Å) boxcar filter for display purposes.

FIG. 2- Sample spectrum (SWP 49555) and spectral fits. The solid line is the observed spectrum, the dotted lines are the spectral components, and the dotted/dashed line is the sum of the components.

FIG. 3- Continuum fluxes in the 1275 Å band. Fluxes from TOMSIPS are plotted as a function of those from IUESIPS in units of 10^{-14} ergs s^{-1} cm^{-2} $Å^{-1}$.

FIG. 4- IUE continuum fluxes in units of 10^{-14} ergs s^{-1} cm^{-2} $Å^{-1}$ are plotted as a function of Julian Date. The fluxes are at the midpoints of the error bars ($\pm 1\sigma$).

FIG. 5- IUE line fluxes in units of 10^{-12} ergs s^{-1} cm^{-2} are plotted as a function of Julian Date. The fluxes are at the midpoints of the error bars ($\pm 1\sigma$).

FIG. 6- Cross-correlation of the 1275 Å continuum band with itself (ACF) and other continuum bands for the continuous data set. The CCF is given by the smooth curve, and the DCF is given by the plotted points and error bars.

FIG. 7- Cross-correlation of the 1275 Å continuum band with itself (ACF) and other continuum bands for the entire data set. The CCF is given by the smooth curve, and the DCF is given by the plotted points and error bars.

FIG. 8- Cross-correlation of the C IV line with itself (ACF) and cross-correlation of the 1275 Å continuum band with the emission lines for the continuous data set. The CCF is given by the smooth curve, and the DCF is given by the plotted points and error bars.

FIG. 9- Cross-correlation of the C IV line with itself (ACF) and cross-correlation of the 1275 Å continuum band with the emission lines for the entire data set. The CCF is given by the smooth curve, and the DCF is given by the plotted points and error bars.

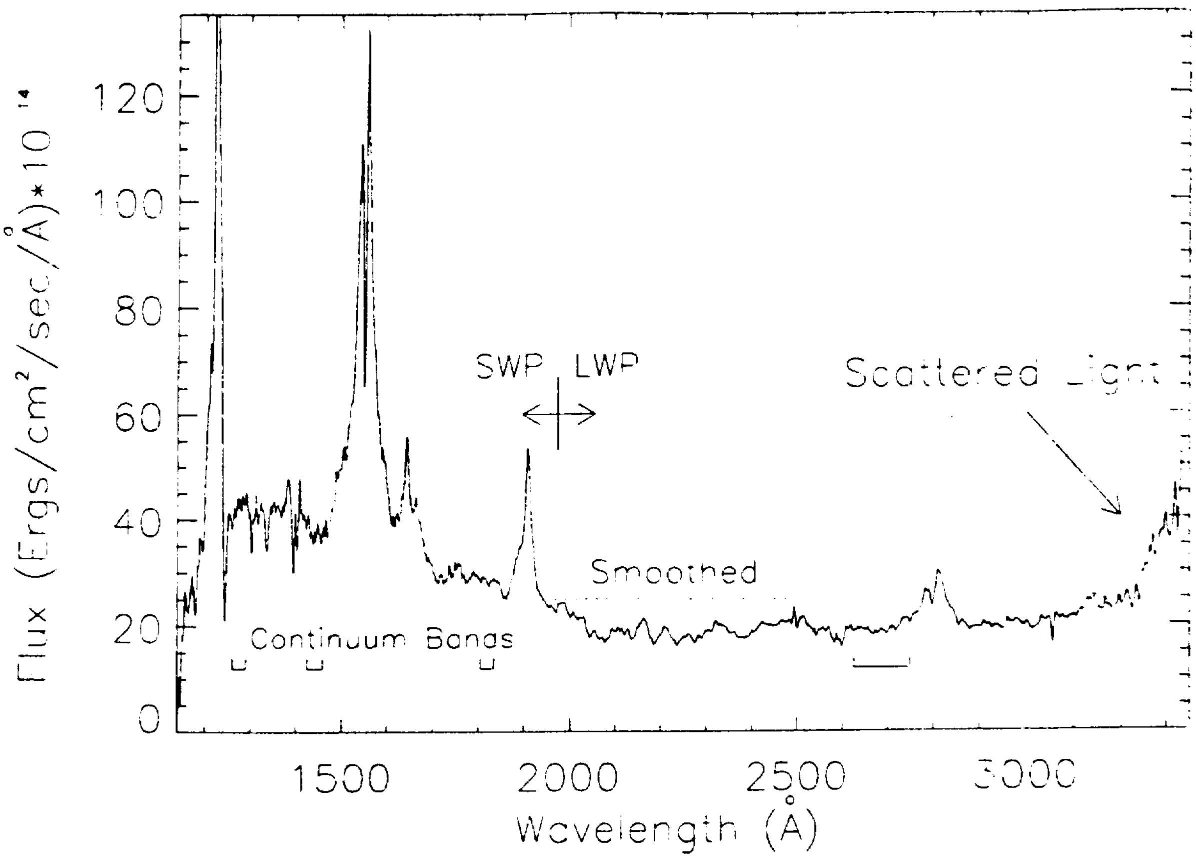

Flux (Ergs/cm²/sec/Å)*10⁻¹⁴
0
20
40
60
80
100
120
1500
2000
2500
3000
Wavelength (Å)
SWP
LWP
Smoothed
Continuum Bands

Figure 1.

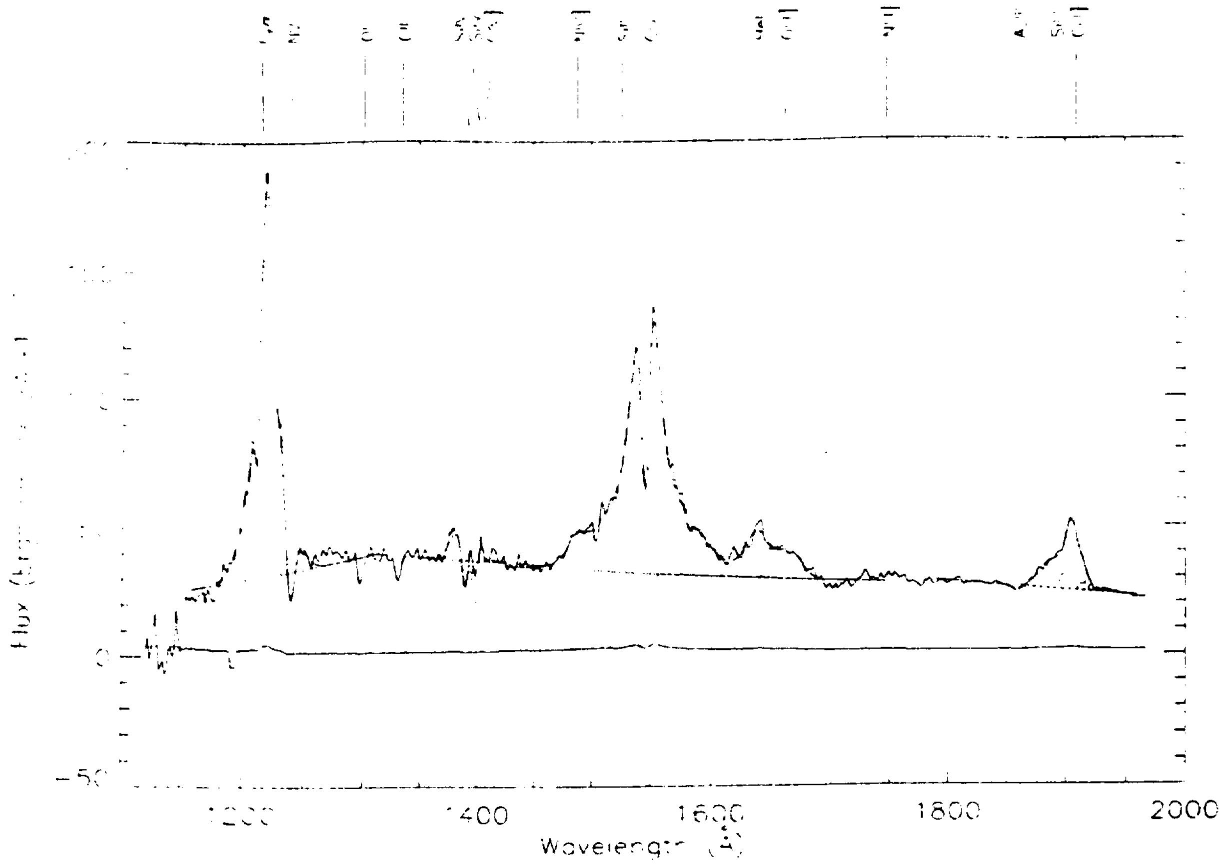

Figure 2.

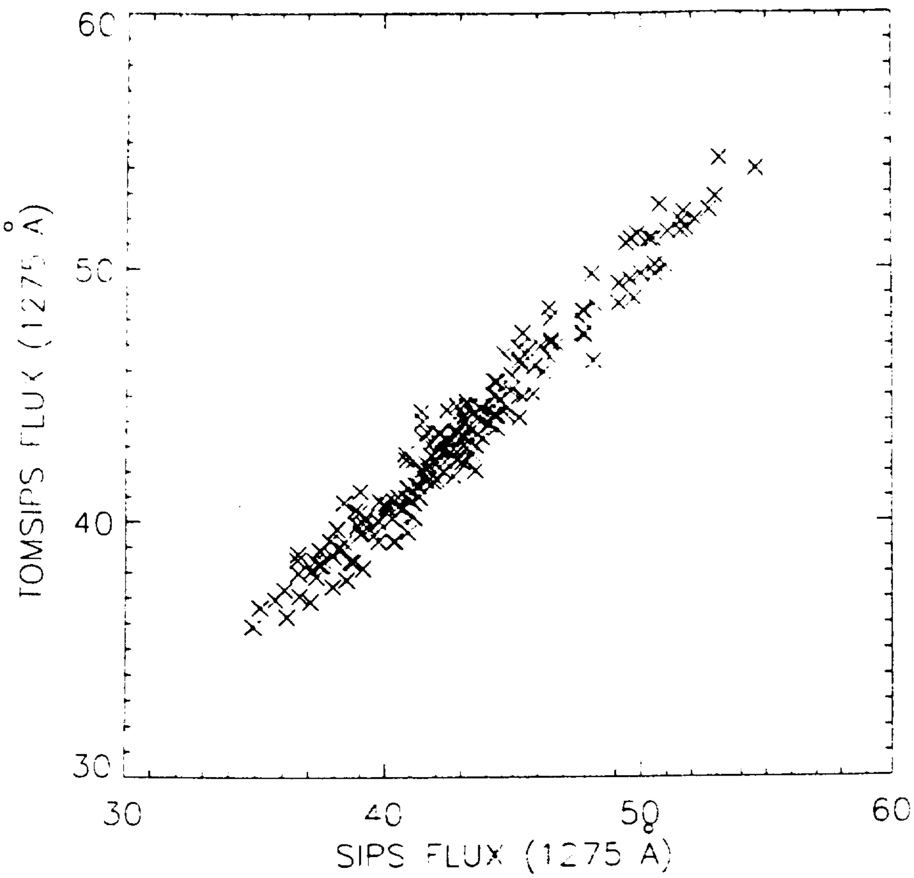

Figure 3.

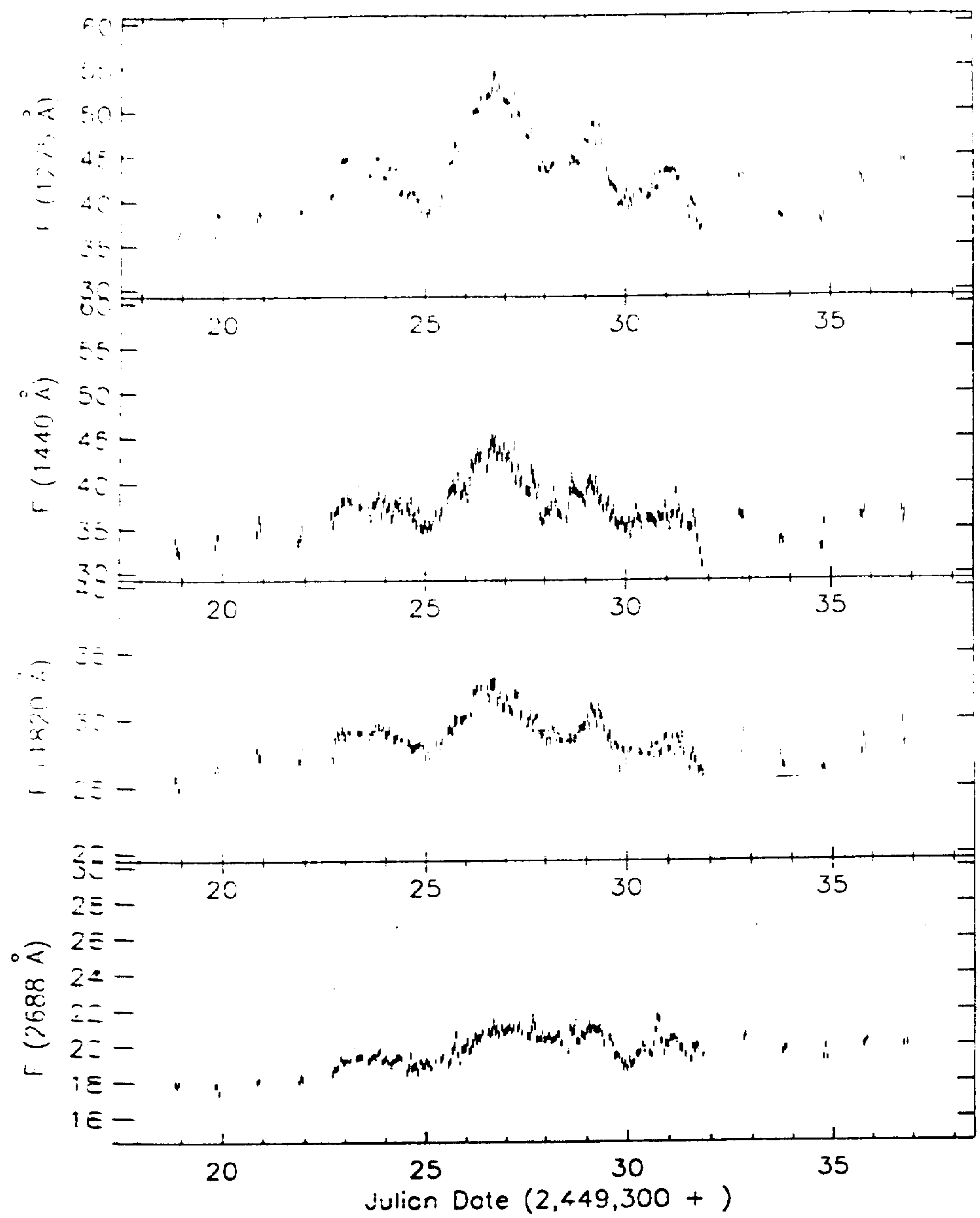

Figure 4.

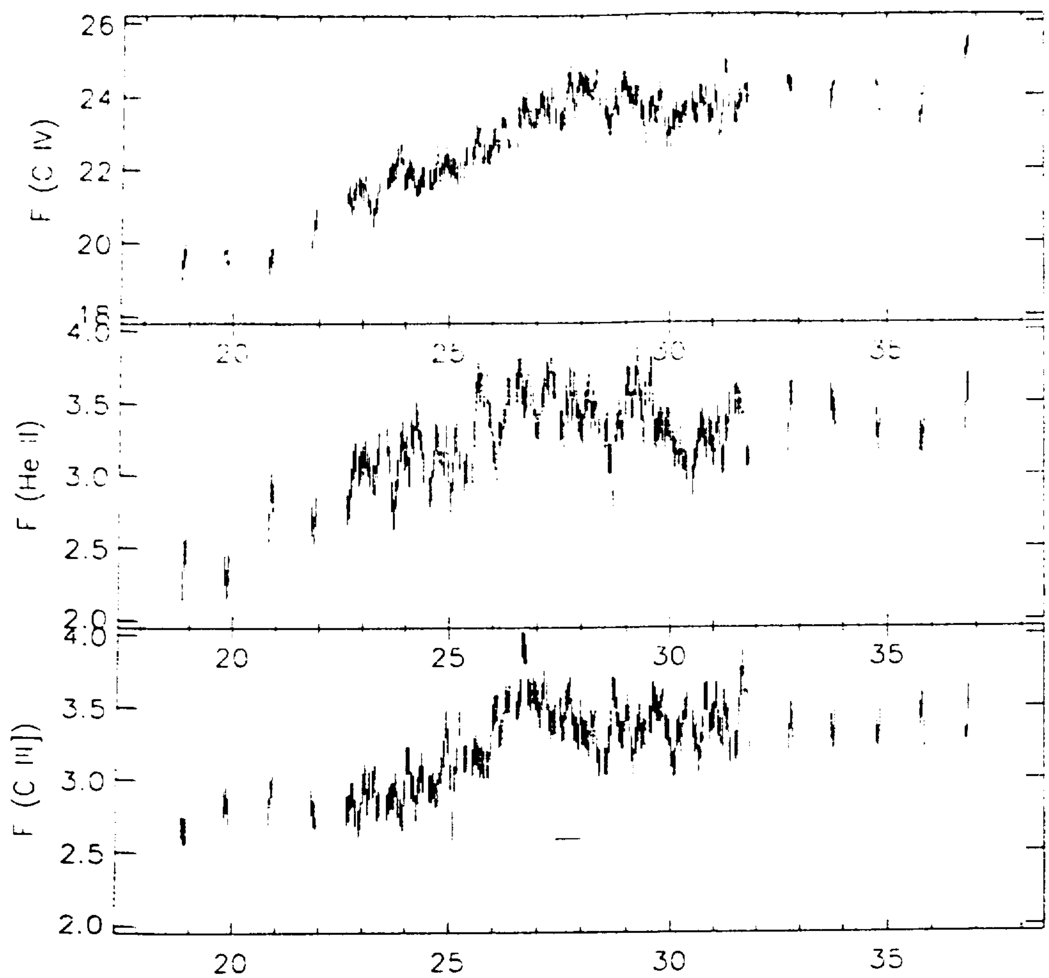

Figure 5.

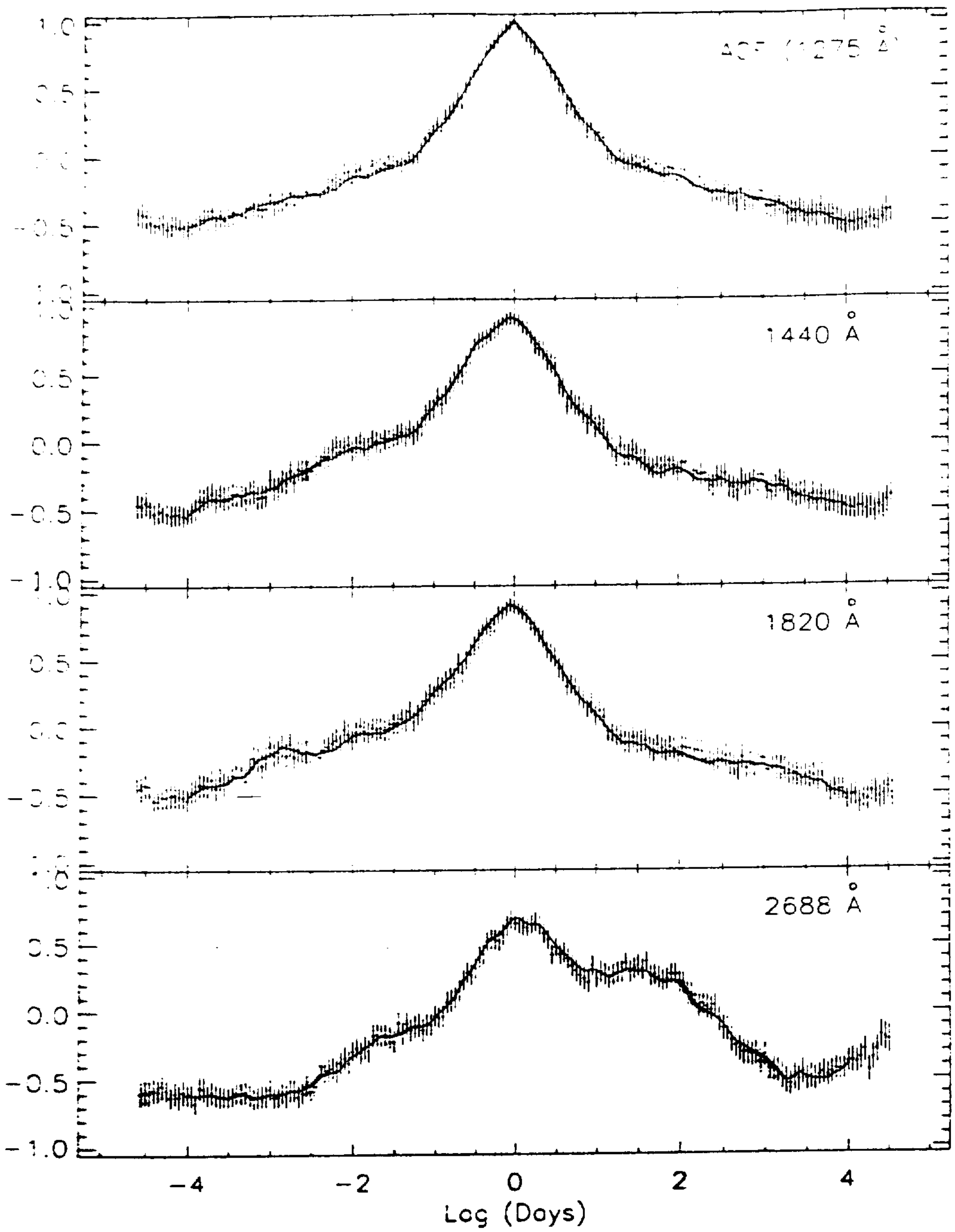

Figure 6.

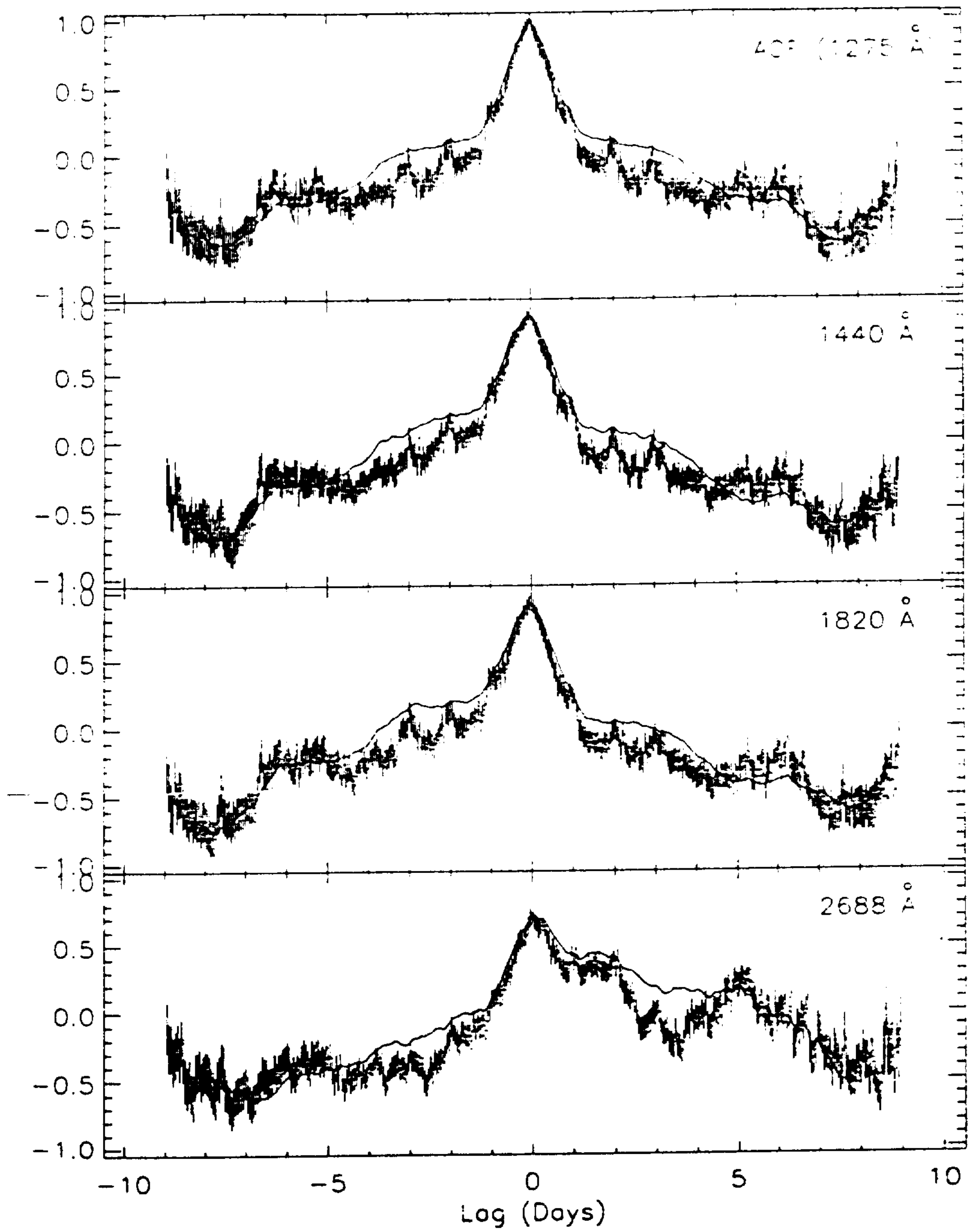

Figure 7.

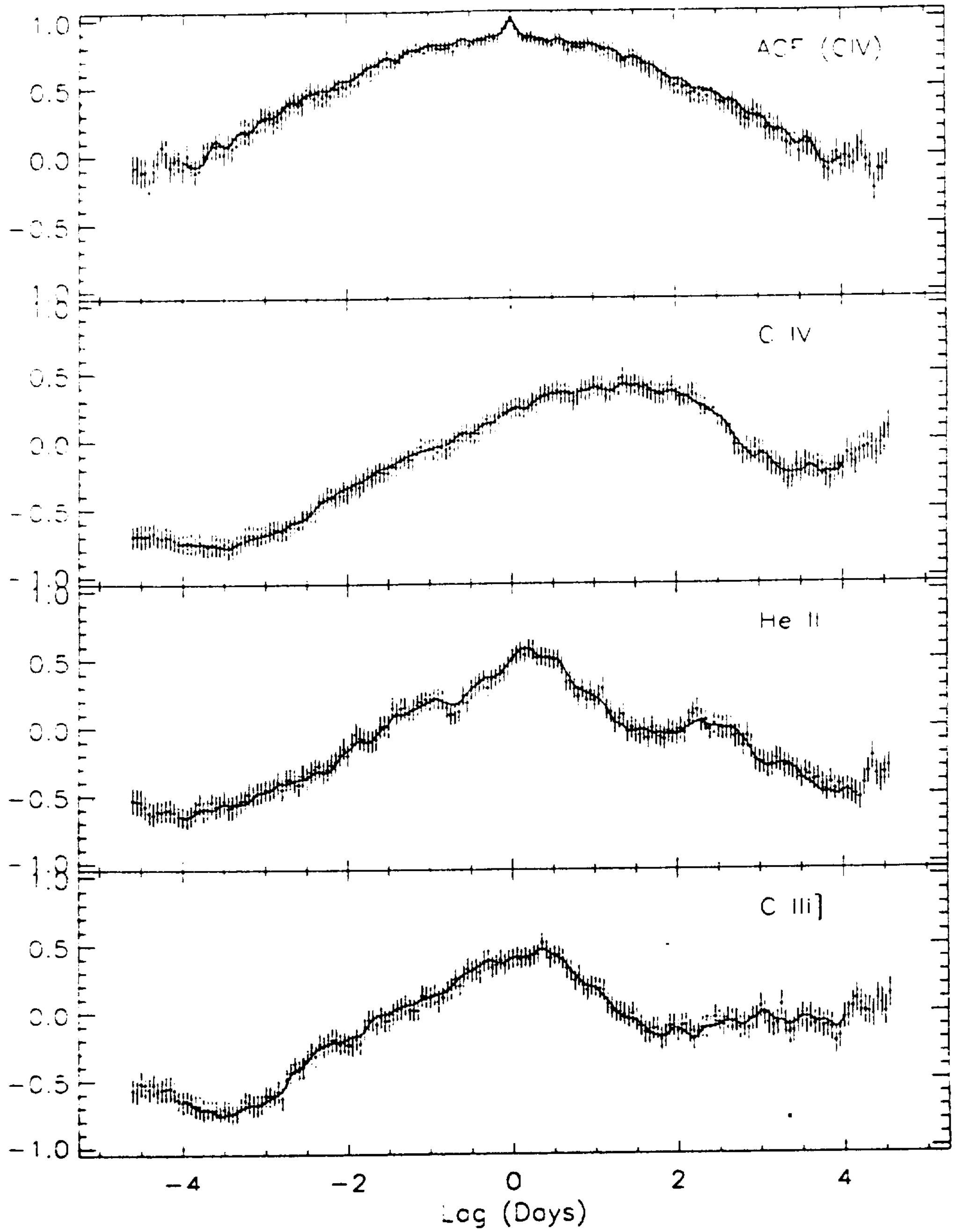

Figure 8.

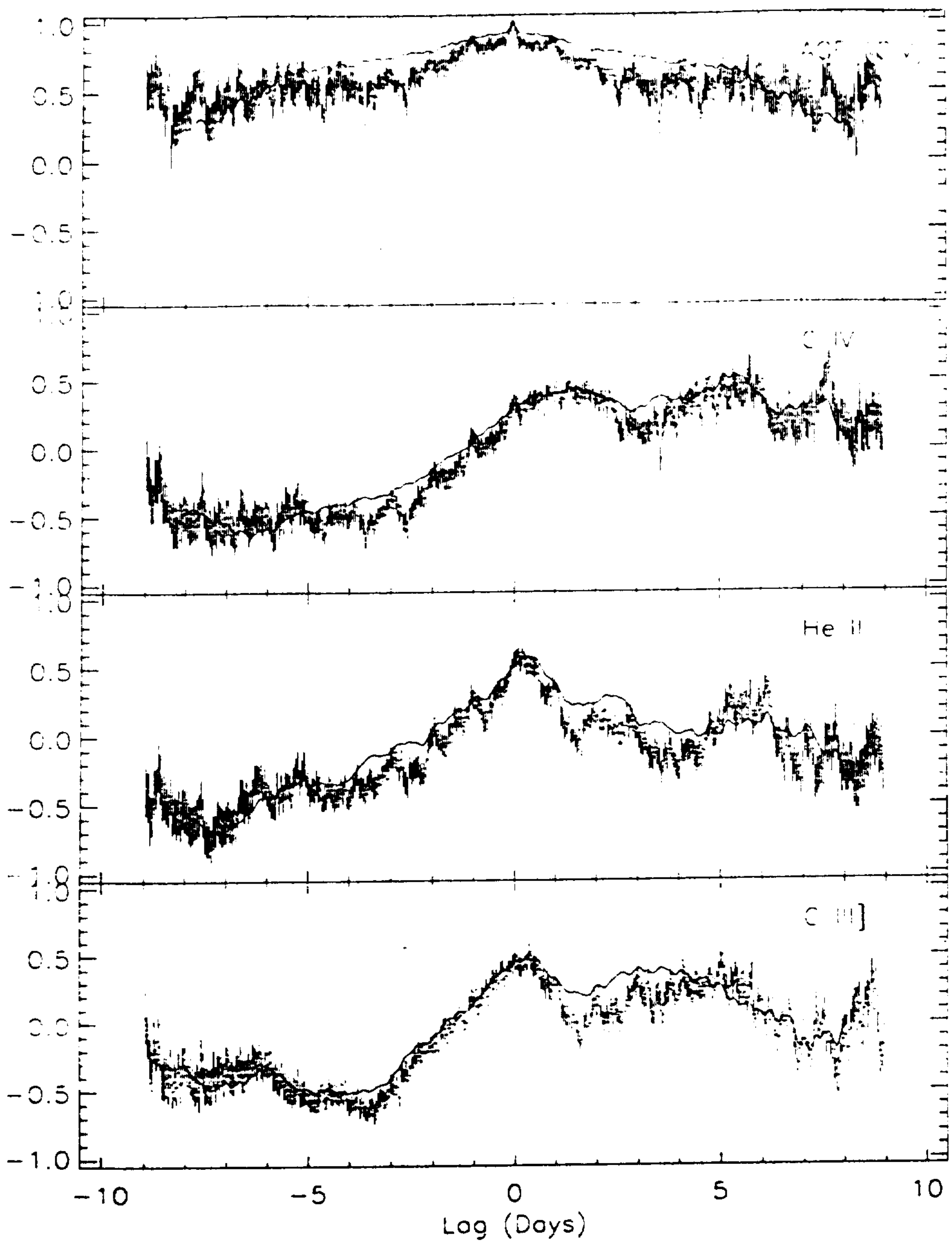

Figure 9.

IN-90- 018195

REPORT DOCUMENTATION PAGE

Form Approved
OMB No. 0704-0188

1. AGENCY USE ONLY *(Leave blank)*

2. REPORT DATE
August 1995

3. REPORT TYPE AND DATES COVERED
Contractor Report

4. TITLE AND SUBTITLE
International AGN Watch: Continuous Monitoring of NGC 4151

5. FUNDING NUMBERS
Code 684.1
Contract: S-30917-F

6. AUTHOR(S)
PI: D. M. Crenshaw

7. PERFORMING ORGANIZATION NAME(S) AND ADDRESS(ES)
Computer Sciences Corporation
4061 Powder Mill Road
Calverton, MD 20705

8. PERFORMING ORGANIZATION REPORT NUMBER
EKNS1170
CAN 4129

9. SPONSORING/MONITORING AGENCY NAME(S) AND ADDRESS(ES)
NASA Aeronautics and Space Administration
Washington, D.C. 20546-0001

10. SPONSORING/MONITORING AGENCY REPORT NUMBER
CR-203634

11. SUPPLEMENTARY NOTES
Technical Monitor: D. West, Code 684.1

12a. DISTRIBUTION/AVAILABILITY STATEMENT
Unclassified-Unlimited
Subject Category: 90
Report available from the NASA Center for AeroSpace Information,
800 Elkridge Landing Road, Linthicum Heights, MD 21090; (301) 621-0390.

12b. DISTRIBUTION CODE

13. ABSTRACT *(Maximum 200 words)*

The results of this project are reported in a 40-page manuscript with over 80 co-authors to be submitted to the Astrophysical Journal. The nucleus of NGC 4151 was observed continuously with the International Ultraviolet Explorer (IUE) for 9.3 days, yeilding a pair of LWP and SWP spectra every 70 minutes, and during four-hour periods for 4 days prior to and 5 days after the continuous monitoring period. The sampling frequency of the observations is an order of magnitude higher than that of any previous UV monitoring campaign on a Seyfert galaxy.

14. SUBJECT TERMS
Astronomy, IUE Research

15. NUMBER OF PAGES
2 plus Appendix

16. PRICE CODE

17. SECURITY CLASSIFICATION OF REPORT	18. SECURITY CLASSIFICATION OF THIS PAGE	19. SECURITY CLASSIFICATION OF ABSTRACT	20. LIMITATION OF ABSTRACT
Unclassified	Unclassified	Unclassified	Unlimited

NSN 7540-01-280-5500

Standard Form 298 (Rev. 2-89)
Prescribed by ANSI Std. 239-18, 298-102